14 Roller Rigs

Weihua Zhang, Huanyun Dai, Zhiyun Shen, and Jing Zeng

CONTENTS

I. Introduction 458
II. The History of Roller Rigs 459
III. The Test Technique and Classification of Roller Rigs 460
IV. Examples of Roller Rigs 462
A. The Chengdu Roller Rig 462
1. Structure of the Chengdu Roller Rig 462
a. Degrees of Freedom of the Rollers 462
b. Components of the Roller Rig 464
i. Test Unit 464
ii. Driving System 465
iii. Hydraulic System 466
iv. Monitoring System 466
v. Data Acquisition and Processing System 466
vi. Auxiliary System 466
c. Function of the Roller Unit 467
d. Curve Simulation 467
2. Characteristics of the Chengdu Roller Rig 469
3. Scope of Test Function 469
B. Naples Roller Rig 470
1. Structure 470
a. Power Supply System 470
b. Overhead Line Simulator 471
c. Roller Test Bench 471
d. Drive and Brake System 472
e. Control System 472
f. Data Acquisition System 473
g. Lifting Equipment 473
2. Function 473
C. The Tokyo Roller Rig (RTRI) 474
1. Roller Unit 474
2. Flywheel Assembly 476
3. Driving Device 476
4. Hydraulic Power Source 476
5. Bogie Holding Device 476
6. Building and Foundations 476
D. The Pueblo Roller Rig (TTC) 476
V. Operation and Results 477
A. Test Methods 477

1. Status of the Test Vehicle 478
2. Status of the Roller Rig 478
3. Stability Test 478
4. Dynamic Simulation Test 479
5. Curve Simulation Test 480
6. Power Test 481
7. Modal Analysis Test 481
8. Storage Security Test 481
B. Differences between Roller and Track 481
1. Differences of Geometry Relationship 481
a. Calculation Method of Wheel–Roller Geometry Relationship 481
b. Geometry Difference of Wheel–Rail Contact and Wheel–Roller Contact 484
2. Difference in Creep Coefficient 487
3. Differences in Stability 489
4. Difference in Vibration Response 491
5. Difference in Curve Simulation 493
C. Influence of Setup Errors on Roller Rig Vehicle Stability 494
1. Diameter of the Rollers 494
2. Gauge of the Rollers 494
3. Cant of the Rollers 494
4. Coefficient of Friction on the Contact Surface 496
5. Vehicle Position on the Roller Rig 496
6. Yaw Angle between Wheelset and Roller Axle 497
D. Examples of Comparison Results with Theoretical Analysis 497
1. Stability Test 498
a. Stability Tests and Theoretical Analysis of a Freight Car 498
b. Stability Test and Theoretical Analysis of a Passenger Car 500
2. Ride Comfort Test and Theoretical Analysis of a Passenger Car 502
VI. Conclusions 504
References 504

I. INTRODUCTION

Experience teaches us that the complete development cycle (design, prototype, railway line tests, industrialisation, production start up, in service adjustment, and corrective action) for a new vehicle featuring a significant level of systems and technological innovation is very time-consuming. The duration and efficiency of prototype experimentation activities is a key element in the development of new rolling stock, and is instrumental in terms of technical and economic success. An awareness of this technological and competitive development has led the railway industry or research institutes to commit extensive financial and technical resources to the creation of test facilities. The main objectives are to reduce the time (and therefore the cost) of testing new vehicles, to make as wide a range of tests available as possible, in order to achieve maximum levels of performance, reliability, and availability in the shortest possible time.

A roller rig is a type of railway vehicle testing plant. First, it is a system capable of testing a vehicle in a running condition without field tests, and second, it allows the study of interaction between a railway wheel and the rail.

The application of roller rigs to the study of vehicle system dynamics and the development of high-speed trains and other railway vehicles has become more widespread in recent decades. Roller rigs are used by researchers and railway organisations around the world to assist in understanding

the behaviour of railway vehicles and developing faster, safer and more efficient railways. Roller rigs have contributed to many current designs of railway vehicles.

Roller rigs have been proved useful for both basic research and development of innovations in suspensions and vehicle components. Full-scale roller rigs offer the advantages that the experiments are independent of weather conditions, individual phenomena can be investigated, and the experiments and the constraints as well as the particular conditions are reproducible.

Full-scale roller rigs have been proven as powerful tools, not only for the demonstration of vehicle dynamics for students, but also for the validation of theoretical work and the test of new concepts of innovative vehicle designs.

II. THE HISTORY OF ROLLER RIGS

Roller rigs were originally used for the investigation of the performance of steam locomotives over 100 years ago. One of the earliest such plants was built at the Swindon works of the Great Western Railway in 1904 (see Figure 14.1).[1–3] The rollers of this rig were moveable and could be adjusted so that the centre of each driving wheel was exactly about the centre of each roller. High speeds could be attained while the engine remained stationary, and a braking arrangement on the rollers measured the traction power of the locomotive at various speeds.

In 1957, a full-scale roller rig with two axles was used at the Railway Technical Research Institute, Japan, which used an eccentric roller to create a sinusoidal excitation. In about 1960, tests of bogies commenced on the newly built full-scale roller rig. This roller rig was put into use for about 30 years and played a very important role in studies related to protection against freight car derailment, regenerative braking, Shinkansen bolsterless bogies, etc. In order to meet the demand for high-speed vehicle tests, a new four-axle, full-scale roller rig with the facility for roller lateral and vertical excitations began construction in 1987.

A roller rig was built in Vitry, France in 1964 by CAFL Company, which allows lateral and vertical motions of the roller on each axle simultaneously using simple hydraulic control methods. By using the roller rig, the vertical, lateral, and yaw vibration frequencies, amplitudes and resonance can be measured. In particular, the influence of the change of the vertical and lateral excitation forces due to the impart force on the vehicle running performance can be studied and the running safety and ride performance can also be investigated.

The roller rig in Berlin, Germany, was built in 1967. This roller rig allows evaluation of traction equipment, acceptance tests for vehicle springs, and assessment of braking systems.

The construction of a roller rig at the BR Research Centre in Derby, began in 1959 and was completed in 1971. This roller rig had the capacity to assess braking power, resonant vibration, and vehicle stability. Latterly, the roller rig has been modified to a modal analysis test stand mainly used for the vibration analysis of vehicle suspension systems.

In 1977, a full-scale roller rig was built in Munich, Germany at Deutsche Bahn AG. The rollers have four degrees of freedom including vertical, lateral, inclination, and rotation. The servohydraulic excitation control system was adopted for the roller rig and can accurately simulate track conditions for the dynamic simulation of a vehicle operating on tracks. The rig is mainly utilised for the measurement of the dynamic performance of vehicles and determination of the effects of vehicle modifications on the system performance. The Munich roller rig has played a very important part in the development of ICE high-speed trains.

In 1978, a roller rig, called the roll dynamics unit, with vibrations applied through the wheels to simulate track conditions, began operation at Pueblo, Colorado, U.S.A. The rig consisted of two separate test stands, one for roller-based testing, and another used as a vibration stand. The rolling stand can be used for hunting stability and traction power simulation tests and the vibration stand used for studies of suspension system features, vehicle system natural frequencies,

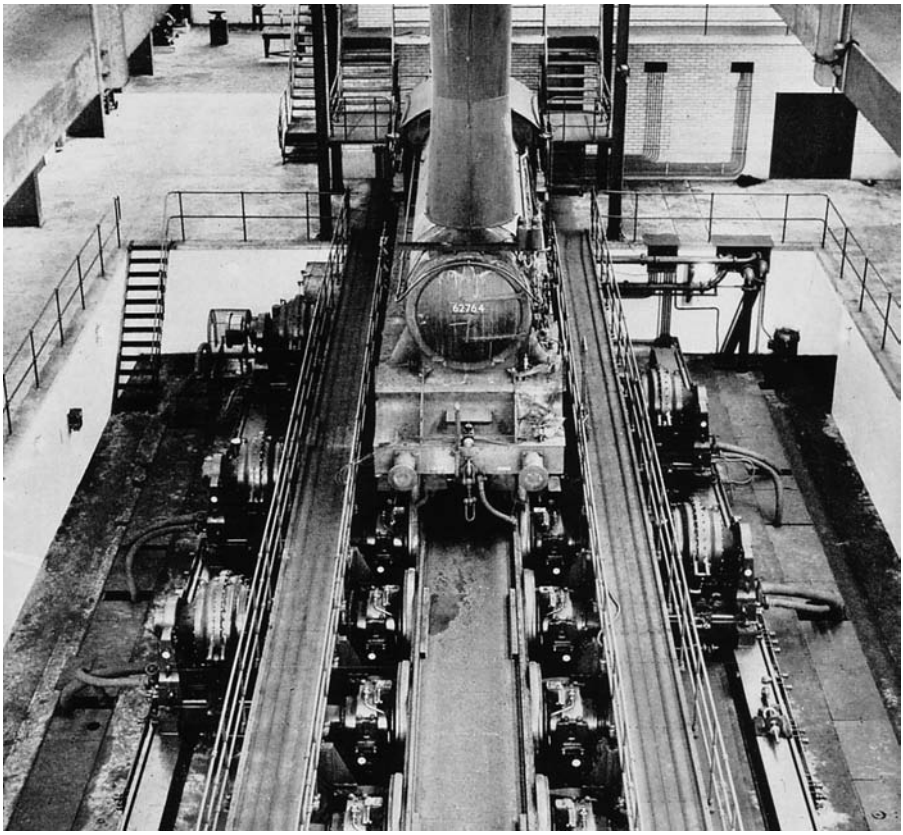

FIGURE 14.1 One of the earliest roller rigs for steam locomotives at the Swindon works of the Great Western Railway.

fatigue strength, and freight load reliability, etc. The rig was designed for speeds of up to 480 km/h.

A roller rig called the curved track simulator was set up at the National Research Council in Ottawa, Canada. It consisted of two pairs of rollers in a flexible frame that permitted the yawing motion of the roller axle to simulate curving. The frame floated on hydrostatic bearings. Unfortunately, the roller rig has since been dismantled.

In 1995, a four-axle roller rig was built at the State Key Laboratory of Traction Power (Southwest Jiaotong University) at Chengdu, China. This roller rig was built for the optimum design and testing of railway vehicles. Each roller can vibrate in lateral and vertical directions. In 2002, two new sets of rollers were added, to form six axles, allowing locomotives to be tested on the rig. In China there are four roller rigs for whole vehicle tests and two rigs for bogie tests. Scale roller rigs have also been used in many research laboratories and this will be discussed in Chapter 15.

III. THE TEST TECHNIQUE AND CLASSIFICATION OF ROLLER RIGS

The main aim of building roller rigs is to provide controlled conditions for investigation and optimisation of railway vehicle performance. The following situations for simulating vehicle operation can be carried out entirely or partly by a roller rig:

- To measure the stability of railway vehicles
- To study wheel–rail interactions

- To simulate the vibration of vehicles running on track with different irregularity conditions
- To simulate the process of train acceleration or braking

A roller rig acts as a track simulator; the rollers with rail profiles form an endless track. It cannot only simulate the running of vehicles on straight track by the rotation of the rollers, but can also simulate track irregularities by the excitation of rollers in a number of axes. When applying rotational resistance to the rollers, the roller rig can provide the traction force to simulate traction and braking effort of a vehicle. Therefore, railway vehicle test facilities can be classified as:

- RTU — a pure rolling roller rig. RTU has the basic function of simulating railway vehicles running on a straight line, with or without traction forces.
- RVTU — a rolling and vibrating roller rig. RVTU not only simulates the vehicles on straight track, but can also simulate track irregularities by the excitation of the rollers, again, with or without traction forces.
- VTU — a test rig using a short vibrating rail under each vehicle wheel, to reproduce track irregularities. The VTU cannot simulate wheel–rail contact and traction power as there is no wheel rolling motion.

Table 14.1 classifies roller rigs from around in the world based on the above groupings. Most are of type RTU. Owing to their combined features, RVTU rigs are inherently more useful in the development of railway vehicles.

The track irregularity shown in Figure 14.2 can be considered to have four components: gauge, cross level, lateral alignment, and vertical profile. When the vertical and lateral disturbances of the left and right rails are indicated as z_L, y_L, z_R, y_R, the four type of track irregularities can be described as:

1. Gauge $= (y_L - y_R)/2$
2. Lateral alignment $= (y_L + y_R)/2$
3. Cross level $= (z_L - z_R)/2$
4. Vertical profile $= (z_L + z_R)/2$

Table 14.2 describes how to use the rollers to simulate track. Ultimately, a roller rig should be capable of simulating track irregularities and also curve negotiation, but to date, there is no rig which is able to simulate both. Only the roller rigs in Munich and in Chengdu possess part curving functions. The roller rig in Munich has now been decommissioned and the roller rig in Chengdu cannot simulate the rail movement along the tangent direction when gauge and lateral alignment irregularities exist. To achieve this function, the rollers must be able to yaw about their vertical axis.

TABLE 14.1
Classification of Roller Rigs

Type	China Chengdu	Germany Munich	America Pueblo	Japan Tokyo	Germany Berlin	Italy Naples	France Vitry	China Qingdao	China Dalian
RTU			✓		✓			✓	✓
RVTU	✓	✓		✓			✓		
VTU			✓					✓	

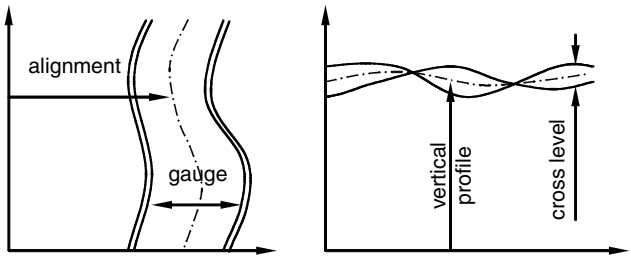

FIGURE 14.2 Track irregularity inputs.

IV. EXAMPLES OF ROLLER RIGS

Roller rigs have been established for many years and the following section details five representative roller rigs that have played an important role in the development of railway vehicles.

A. The Chengdu Roller Rig[4,5]

China has more than 70,000 km of railway line. The service speed of passenger trains on main lines has risen from approximately 50 to 70 km/h in the 1980s to approximately 140 to 160 km/h in the 1990s. This rise in vehicle speed has been mainly attributed to the use of test facilities, especially roller rigs. The successful application of these rigs within China has resulted in a growth in their use. There are now six roller rigs in service, but only the roller rig in Chengdu has function of rotation and vibration combined together.

The roller rig in Chengdu was developed by the State Key Laboratory of Traction Power (Southwest Jiaotong University). Each roller can move in vertical and lateral directions independently under servo control. Design of the roller rig began in 1989 and it came into service in 1995. From 1995 to 2005 more than 50 railway vehicles were tested. The original roller rig had four roller sets (allowed testing of up to four-axle vehicles) with the two rollers of each set constrained to have the same rotational speed. These constraints meant the roller rig could only simulate a four-axle vehicle running on straight track, with a maximum gauge variation of between 1435 and 1676 mm. As the rig was heavily utilised in the development of new railway vehicles, it was extended to six roller sets and the structure improved during 2002. Four roller sets of the new modified rig have the ability of gauge variation of between 1000 and 1676 mm and the two rollers of each roller set can be run at different rotational speeds. This roller rig is shown in Figure 14.3.

1. Structure of the Chengdu Roller Rig

a. Degrees of Freedom of the Rollers

An ideal roller rig should have the degrees of freedom as described in Table 14.2. In reality, considering design, manufacturing, and financial constraints, the most useful of the described degrees of freedom were chosen. The degrees of freedom of the Chengdu roller rig are shown in Figure 14.4:

- Movement of the two rollers independently in the Y direction simulates the track irregularities of gauge and lateral alignment.
- Movement of the two rollers independently in the Z direction simulates the track irregularities of cross level and vertical profile.
- Turning of the two rollers about the X axis is to simulate the cant angle in curving.

TABLE 14.2
Relationship between Status of Rails and Rollers

No.	Type of Irregularity	Status of Rails	Status of Rollers	Remark
1	Cross level	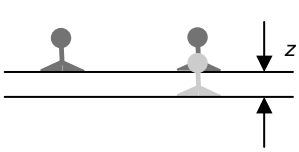	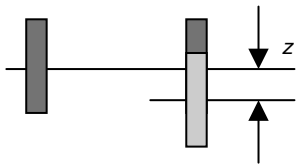	Left roller and right roller move relatively vertically
2	Vertical profile	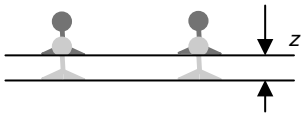	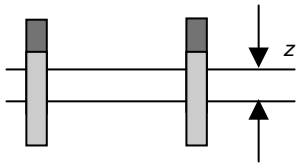	Left roller and right roller move synchronously vertically
3	Alignment	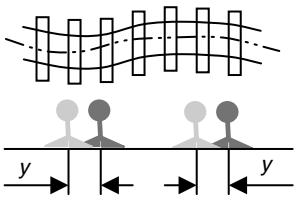	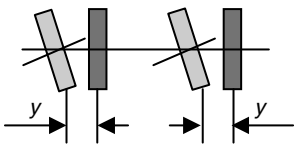	Left roller and right roller move in lateral and yaw directions
4	Gauge	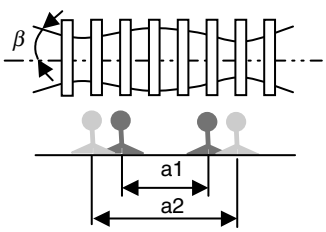	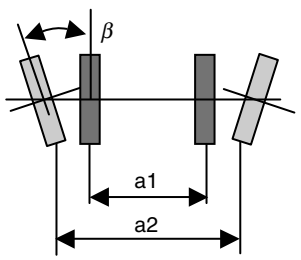	Left roller and right roller move in lateral relatively and corresponding yaw motion
5	Curve	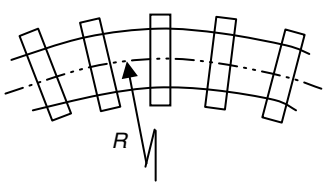	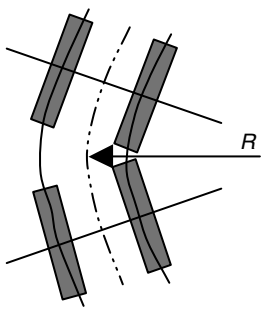	Left roller and right roller are set in curved position and rotate at different speeds
6	Cant in curve	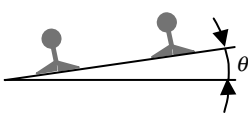	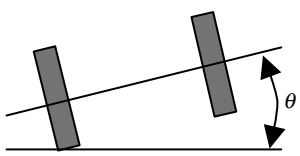	Left roller and right roller tilt synchronously

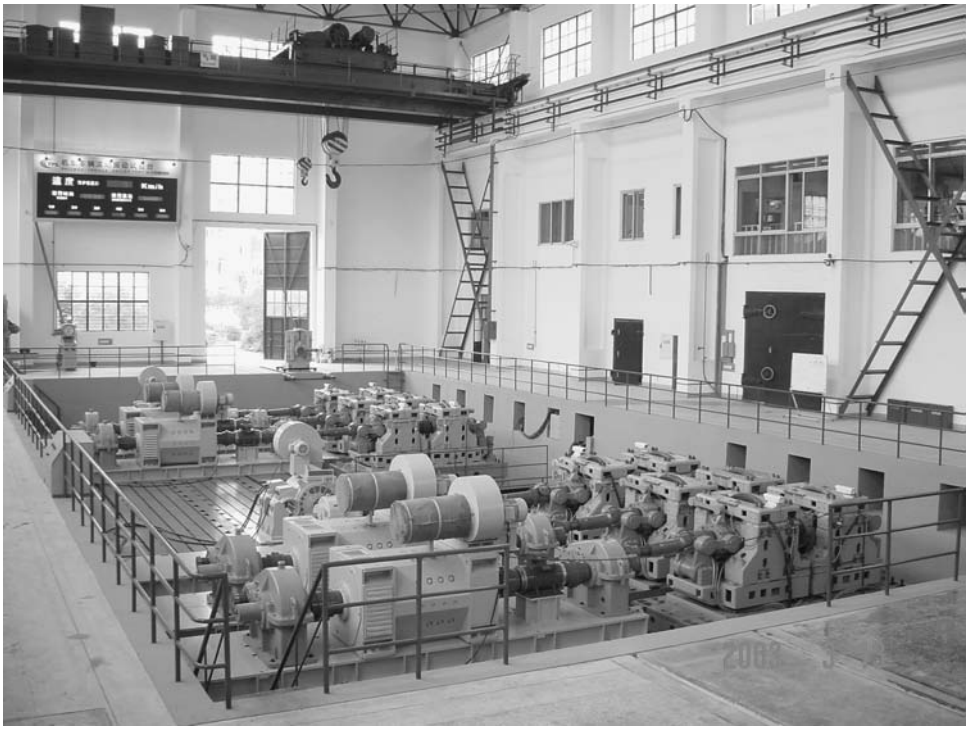

FIGURE 14.3 The roller rig in Chengdu (without flywheel).

- Rotation of the two rollers at the same speed about the *Y* axis is to simulate the forward speed of vehicle on straight track, and with different speeds is to simulate curving.
- Turning of the two rollers about the *Z* axis allows simulation of the track tangent in a curve.

The linear motions of the two rollers in the *Y* and *Z* directions and also the rotation of the two rollers about the *Y* axis are controlled during the roller rig operation. The rotation about the *X* and *Z* axes is applied only for curve simulation which is preset before the test. That is, this roller rig can simulate straight track and circular curved track with track irregularities.

b. Components of the Roller Rig

Hydraulic actuators provide the movements of the two rollers in *Y* and *Z* directions, and the rotation about the *Y* axis is driven by the motor. The roller rig is composed of several subsystems including the test unit, driving system, hydraulic system, monitoring system, and data acquisition and processing system. The whole test system of the roller rig is shown in Figure 14.5. The main power supply for the rig comes from the railway power supply with 25 kV and 50 Hz or a low-level power supply of 380 V at 50 Hz.

i. Test Unit

The roller rig has six test units. They are independent and can be moved according to different vehicle configurations. Each test unit consists of a roller unit and a driving unit, as shown in Figure 14.6. The driving unit can provide different rotational speeds and torque to the rollers, via a double-articulated universal joint, according to the task required. Within the driving unit, there is a DC motor, two

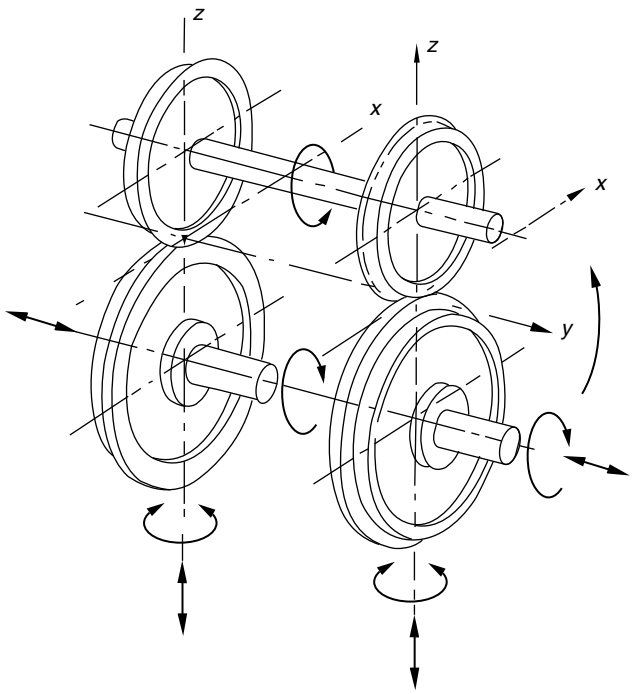

FIGURE 14.4 Freedom of the rollers.

gearboxes, a flywheel, and a torsion meter, all fixed to a welded frame. The motor can work as a driving motor or a generator according to the requirement of driving or braking. The flywheel is used to maintain the running stability of the roller rig and to simulate the inertia of the vehicle. Gearbox II is used to accelerate the flywheel, while gearbox I is used to apply different rotational speeds and torques by setting the transmission ratio as 1:1, 2:1 (for high torque) or 1:2 (for high speed).

ii. Driving System

The driving system consists of a remote control computer, digital controller, converter, motor excitation, resistance, and motor. Using a feedback control technique, the operator can control the motor operation according to the defined running speed or operating torque through the remote

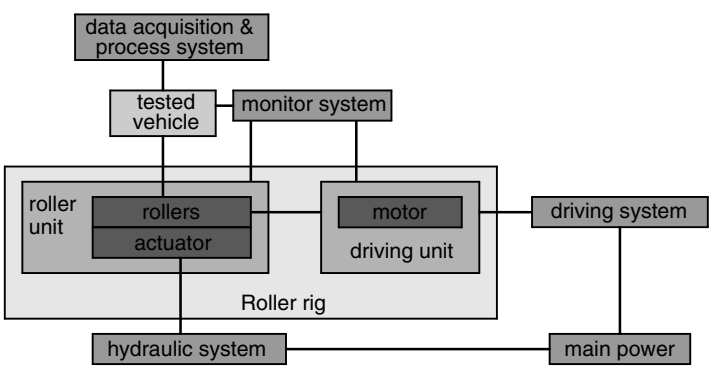

FIGURE 14.5 System of roller rig.

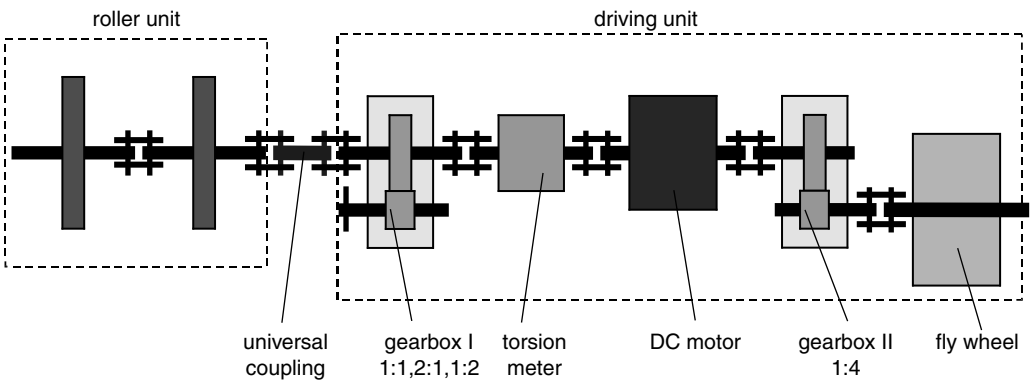

FIGURE 14.6 Test unit.

control computer. The maximum difference between the rotation speeds of the six test units can be controlled within 0.5%. Therefore, the driving system can ensure that the six roller sets are rotating almost synchronously without any mechanical connection.

iii. Hydraulic System

The movements of the rollers in the vertical and lateral directions are provided by the lateral and vertical hydraulic actuators; the roller rig is a complicated system with a total of 24 actuators for the 12 rollers. By using the digital controller, motion of the actuators is controlled by displacement-based PID feedback control.

iv. Monitoring System

The operation of the roller rig is surveyed by a monitoring system. The monitoring system can display the roller rig running speed and torque, temperature of bearings, and lubricating oil. Through the 12-channel video system, the status of the roller rig and the tested vehicle, the contact condition of roller and wheel can be monitored. The system also has the function of overload protection and safety interlocking.

v. Data Acquisition and Processing System

According to the railway vehicle test evaluation standards, the responses of the tested vehicle should be recorded during the test. The data acquisition and processing system can measure the signals of displacement, velocity, acceleration, strain, pressure, temperature, voltage, current, etc. All signals can be measured, conditioned, and sent to the acquisition computer via a network link. Up to 200 channels of data can be acquired.

The terminal operating computers for the driving system, hydraulic system, monitor system, and data acquisition and processing system are arranged on a desk in the control room, as shown in Figure 14.7.

vi. Auxiliary System

The following are auxiliary facilities of the roller rig:

- Test shed — the test shed with a length of 72 m and width of 24 m is divided into two sections, one section is for the roller rig, the other for test preparation and locating facilities for component tests.
- Component test stands — vehicle suspension parameter measurement, fatigue test, etc.
- Power supply — there are two power supply systems. The civil power system with three-phase AC 10 kV is used for the driving motors of the roller rig. The hydraulic system and

FIGURE 14.7 The control room.

other systems use 380 V. The railway power system of AC 25 kV is to power locomotives under test.

- Crane — there are two gantry cranes in the test shed with capacity of 50 t each.

c. Function of the Roller Unit

The roller unit is the key part of the roller rig. A schematic of the roller unit of the Chengdu rig is shown in Figure 14.8. The roller is supported by a U-shaped frame via a pair of roller bearings. The rollers can rotate within the U-frame via a universal coupling. The rollers, together with the U-frame, can move in a vertical direction using the hydraulic actuators. The shaft of the roller is fixed within a bearing housing, which can be pushed or pulled through a lever arm by a hydraulic actuator. The upper part of the roller unit is installed on a subframe, which can rotate via a ring bearing, that allows rotation through a predefined angle to suit a simulated curve radius. The left and right rollers can be moved independently; a gear coupling allows the transfer of rotational torque and variation in drive speed of the left and right rollers. The subframe also allows the upper part of the roller unit to tilt using a lift actuator to simulate the cant angle of a curve. The whole roller unit is seated on a base frame, which allows longitudinal movement to accommodate variation in vehicle wheelbase.

d. Curve Simulation

A special characteristic of the Chengdu roller rig is that the left and right roller can rotate at different speeds, which means the roller rig can simulate a wheelset in a curve. This function is realised by a complicated differential driving system. The principle of the differential driving system for one test unit is shown in Figure 14.9. It can be seen that there is no direct coupling between the left and right roller. The motor drive is divided into two by the cone gear in gearbox I.

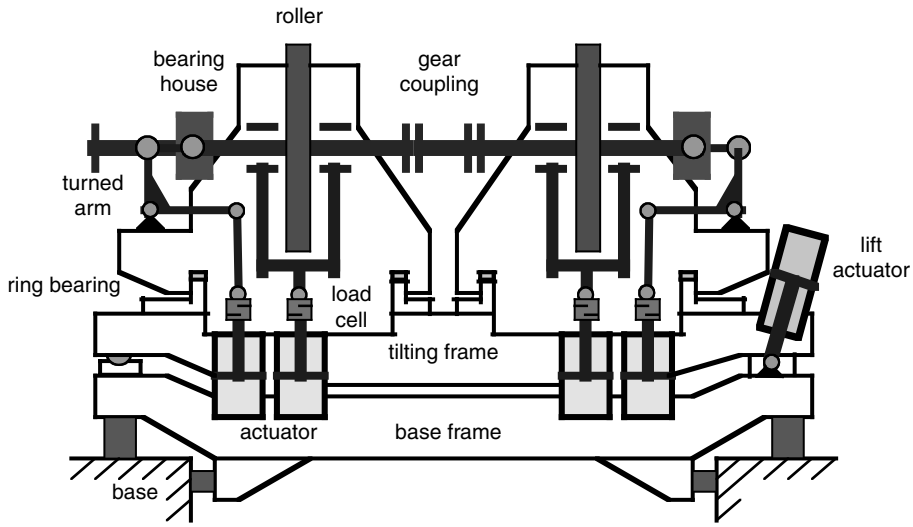

FIGURE 14.8 Sketch of Chengdu roller unit.

One gear takes drive directly to the right roller through a shaft and universal coupling. Another drive is transferred to the cone gearbox II and then to the differential gearbox. When the drive passes through the differential gearbox, the speed of input shaft can be different from the speed of the output shaft according to the speed of the differential speed motor. The modified drive speed is then transferred to the left roller through cone gearboxes III and VI. This allows the left roller to run with the same rotational direction as the right roller but at a different speed to simulate the speed differential between left and right wheels during curving. Figure 14.10 shows a picture of the roller rig components for simulating curve negotiation.

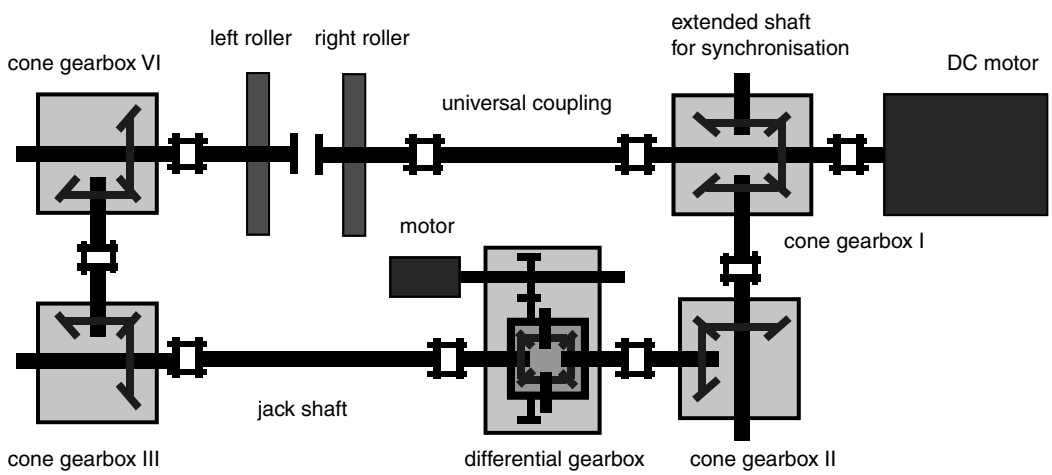

FIGURE 14.9 Sketch of differential driving system.

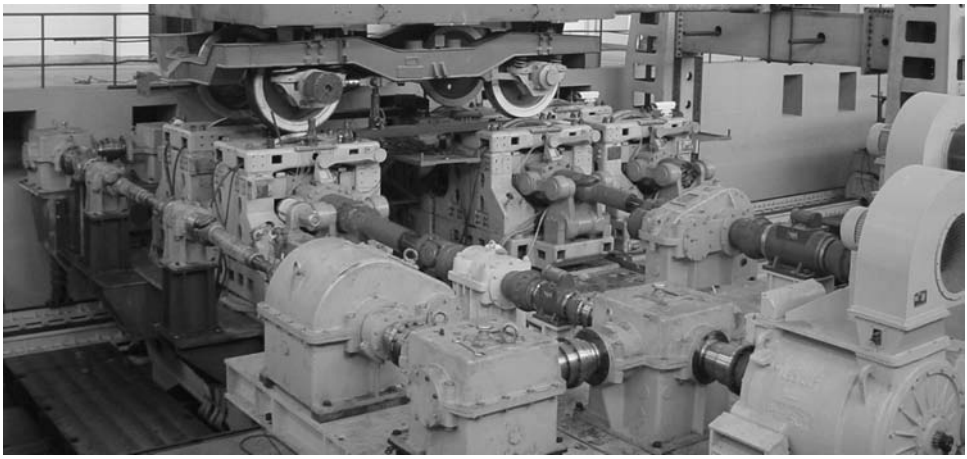

FIGURE 14.10 The roller rig with differential driving system.

TABLE 14.3
Main Characteristic Parameters of Chengdu Roller Rig

Exciting in Vertical		Exciting in Lateral	
Maximum Frequency f_{vmax}	30 Hz	Maximum Frequency f_{vmax}	30 Hz
Maximum Amplitude A_{vmax}	± 10 mm	Maximum Amplitude A_{hmax}	± 10 mm
Maximum Acceleration a_{vmax}	± 4 g	Maximum Acceleration a_{hmax}	± 5 g
Maximum traction force per axle F_e	10 T	Maximum axle load Mw	25 T
Maximum motor power/brake W	1200/1500 kW	Maximum speed V	450 km/h
Maximum cant angle ϕ_{max}	7°	Distance between bogies L	4 ~ 22 m
Bogie wheelbase l	1600 ~ 3500 mm	Range of gauge A_0	1000 ~ 1676 mm
Minimum curve radius R	200 m	Maximum wheelset numbers Nz	6

2. Characteristics of the Chengdu Roller Rig

The main parameters of the roller rig are shown in Table 14.3. The rig can test conventional four-axle and up to six-axle railway vehicles. The roller rig can run in either active or passive mode for vehicle testing depending on whether testing a locomotive or unpowered trailer car.

3. Scope of Test Function

The Chengdu roller rig is not only used to verify the performance of railway vehicles, but also for basic research duties, such as wheel–rail contact mechanics, wear, noise, etc. Its main functions are listed below:

1. Basic research on wheel–rail creep theory
2. Study of derailment mechanisms
3. Hunting stability
4. Dynamic response and ride comfort
5. Curve simulation and operating safety
6. Vibration, mode shape, dynamic stresses of railway vehicles and their components
7. Goods load safety

8. Driving or braking power tests and optimisation of train operation
9. Wheel–rail wear, adhesion and control
10. Wheel–rail interaction forces and the forces on components of vehicle systems
11. Wheel–rail noise and noise reduction
12. Static and dynamic parameter measurement of railway vehicle systems

B. Naples Roller Rig[7–9]

The roller rig at the Ansaldo Transport Research Centre in Naples, Italy, was competed at the end of 1992. Initially, the roller rig has been configured with four rollers (axle), but is designed to allow future upgrading to test six-axle vehicles. The rig is mainly used to test railway locomotives for traction simulation. Its rollers can only rotate about the *X*-axis to simulate running on straight track. Figure 14.11 shows an overview of the Naples roller rig. The rig allows the testing of vehicles with the following characteristics:

- Total weight (max.) of a four-axle vehicle (25 t/axle, 250 km/h) 100,000 kg
- Wheel diameter 500–1400 mm
- Maximum traction effort per axle 100 kN
- Maximum speed (22 t/axle with 1500-mm diameter rollers) 300 km/h
- Range of gauges available 600–1700 mm
- Bogie wheelbase 1400–3500 mm
- Distance between bogies (four-axle vehicle) 5200–22,000 mm
- Maximum continuous power at the axle 1500 kW

1. Structure

The Naples roller rig is basically composed as follows.

a. Power Supply System

Since the power supply of railway systems in Europe varies, the difference not only being voltage but also current (AC or DC), the power supply system of the Naples roller rig is flexible.

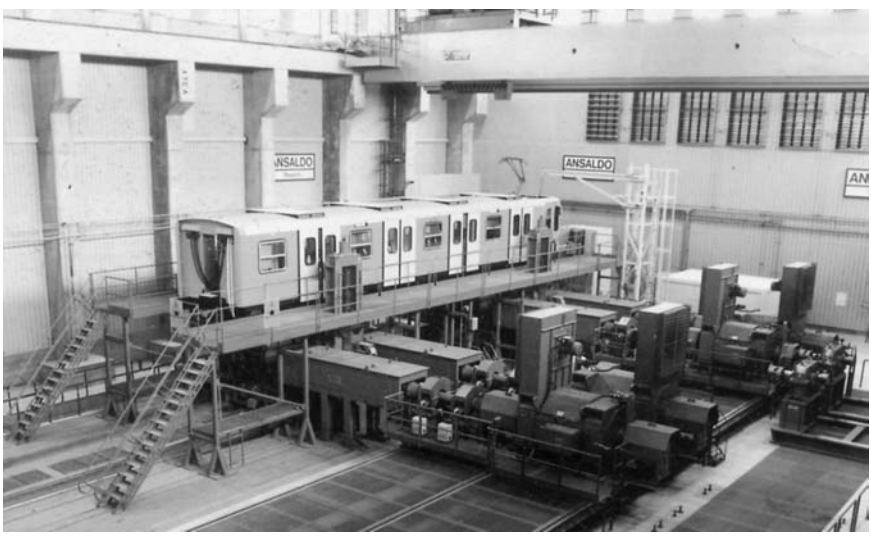

FIGURE 14.11 Overview of the Naples roller rig.

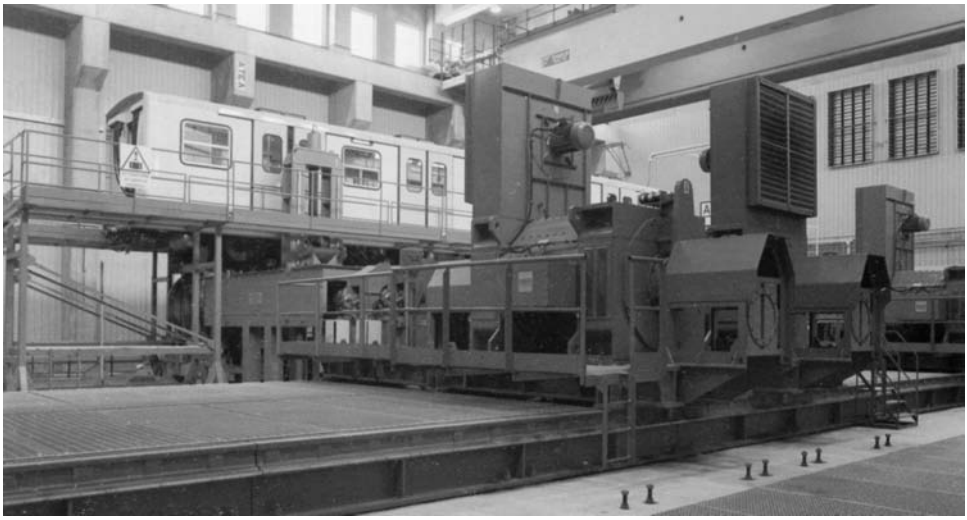

FIGURE 14.12 Overview of drive and brake systems of the Naples roller rig.

The primary power is ENEL (Italian National Power Utility) power. Using a 60/9 kV transformer, the ENEL power transforms to 9 kV using a three-phase bus bar in the power room. The power used for locomotives is 25 kV, 50 Hz or 15 kV, $16\frac{2}{3}$ Hz; they are drawn from the 9 kV bus bar (Figure 14.12).

b. Overhead Line Simulator

Power is fed to the test locomotive through its own pantograph. The real field power supply is characterised by:

- A no-load voltage at the current terminal point which varies on the basis of absorption by other vehicles
- Power supply system equivalent resistance and inductance which vary as a function of vehicle position
- Limited maximum power during recovery

The overhead line power supply control system makes it possible to reproduce the above conditions in the test facility (programmable). Depending on the tests to be performed, the following types of overhead line power feeding system controls are possible:

- Power supply in stable condition
- Power supply in variable condition
- Power supply with voltage jumps
- Power supply with line section simulation (programmed as a function of the distance covered by the vehicle during simulation)

c. Roller Test Bench

This is the main part of the railway vehicle test facility. The rollers are fixed on an axle. Normally, the gauge of two rollers on one axle is 1435 mm. To test vehicles with different gauge, rollers must be exchanged with other rollers from a "roller park." Each of these rollers is mechanically

connected to an electrical machine regulated to deliver a resistant torque with an amplitude and sign which varies on the basis of the dynamic train behaviour.

d. Drive and Brake System

The drive and brake system is of a DC type and suited to the typical operation of each traction motor. Each roller is connected to a generator/motor. The roller drive control functions are as follows:

- Speed control
- Torque control
- Synchronous roller speed control

Speed and torque control are available for synchronous roller speeds. The driving system guarantees precision of the order of 0.1%.

When the motor works as a generator, the power will be recovered and directed back to the 9 kV bus bar, a bidirectional conversion section is used. The converters are very powerful; the main characteristics of one converter are 1600 kW, 750 V, 0/230/1065 rpm. This roller rig motor connects directly to the roller axle without a gearbox or braking device.

e. Control System

System automation is based on the distributed intelligence structure used for industrial process control. The control system, shown in Figure 14.13, comprises two levels. Level I, shown in Figure 14.14a, is the installation's basic automation and comprises:

- One test facility control desk (Figure 14.14b) — all functions indicated in OIS paragraph, signalling, and emergency control
- One locomotive control desk (Figure 14.14c) — vehicle initialisation, manual command entry, locomotive status display, and emergency control
- One mobile supervision desk — test facility operating status display, reference display for manual operation
- Four programmable logic controllers (PLC) — Data acquisition from the plant and vehicle/drives under test, control logic implementation, protection logic implementation

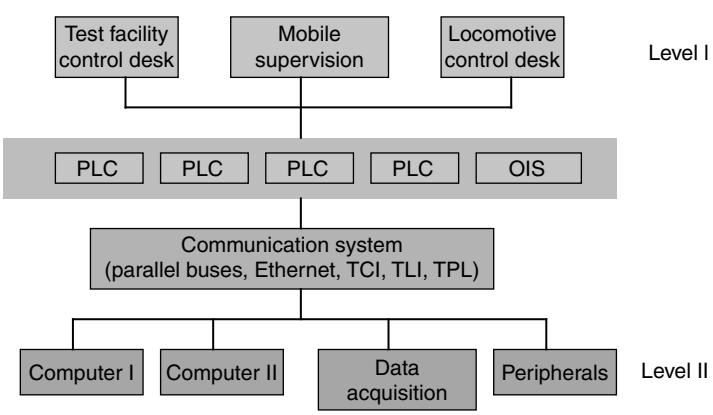

FIGURE 14.13 Control system.

FIGURE 14.14 Control system: (a) level I of control system; (b) test facility control desk; (c) locomotive control desk.

- One operator interface system — configuration of plant video pages, configuration of basic plant data, selection of remote initialisation mode for test facility, remote control and status display of circuit breakers and disconnecters, manual command entry, test mode display, monitoring of data from test facility and test item, alarm display and printout

Level II is used to perform general plant control and supervision. Two computers with relative peripherals perform the following function:

- Computer 1 — control and supervision
- Computer 2 — development and backup

f. Data Acquisition System

This system acquires signals from the test vehicle during testing and can receive up to 400 signals, including high frequency and high voltage signals (1 MHz, >1 kV), medium frequency signals (<50 kHz), low frequency signals (<1 kHz), and temperature signals. This structure includes:

- A computer with relative peripherals — data storage, data processing, data display
- Acquisition cards — A/D conversion
- Interface equipment — signal conditioning

g. Lifting Equipment

In order to position the vehicle on the rollers, two 160 tonne twin-bridge cranes operating in tandem are available. Four electromechanical jacks are also provided to lift the test vehicle and ensure prefect alignment between the wheel axes and the corresponding roller axes.

2. Function

The Naples roller rig is a successful vehicle test facility for power testing. The test type can be short duration tests, long duration, or series of tests. A few examples of tests performed are described as follows:

1. Standard start-up test — the aim is to study the behaviour of vehicles in various start-up condition covered by specification and to verify the global vehicle traction effort, traction effort during transients, and speed as a function of time.
2. Standard simulated path test — the aim is to simulate the motor car (locomotive) running from station to station. The characteristics of the path, such as height profile of the line, radii of curvature, speed limits, tunnels, stops, no load voltage, are simulated.

3. Standard braking test — the objectives are verification of the electrical braking effort of the vehicle as a function, electrical and pneumatic braking effort, and speed.
4. Standard line voltage step variation test — the objectives are verification of vehicle operating continuity during traction and braking, verification of traction and braking effort continuity, and verification of performance with undue intervention of the vehicle protection devices.

C. The Tokyo Roller Rig (RTRI)[10,11]

The roller rig at the Railway Technical Research Institute (RTRI) of Japan was built in 1957 and has contributed greatly to research and development including the high-speed bogies used for the Shinkansen trains, countermeasures against derailment of freight cars, regenerative braking, and bolsterless bogies, and has also played an important role in technical cooperation with domestic and overseas railways. However, the old plant was becoming outdated and its functions limited, as 30 years have passed since its completion. It had become difficult to operate from the viewpoint of noise and vibration to the surrounding area. After 30 years of operation the plant was renewed with respect to the requirements of future railway vehicle development. The new facility was brought into operation at the end of 1989 (see Figure 14.15).

The general arrangement of the roller rig is shown in Figure 14.16. The maximum testing speed of the new roller rig is 500 km/h. One of the major additions to the rig was the facility for inducing vibrations using actuators.

The principal devices in the plant are outlined below:

1. Roller Unit

Gauge	1,000 ~ 1676 mm(variable)
Minimum wheelbase	1600 mm
Maximum test speed	500 km/h
Maximum axle load	200 kN
Diameter of roller	1500 mm
Lateral displacement	0 ~ 1 Hz Max. ± 30 mm
	3 Hz Max. ± 10 mm
	10 Hz Max. ± 2 mm
	Maximum acceleration 10 m/sec^2
Vertical displacement	0 ~ 1.8 Hz Max. ± 12 mm
	25 Hz Max. ± 0.4 mm
	Maximum acceleration 10 m/sec^2
Rolling displacement	0 ~ 2 Hz Max. ± 0.011 rad
	15 Hz Max. ± 0.0006 rad
	Maximum acceleration 5 rad/sec^2

The principal functions of this plant consist of rollers on which the bogie is tested, hydrostatic bearings, hydrostatic couplings, actuators for lateral vibration, movable beds, etc.

A set of rollers and shaft assemblies is supported by hydrostatically controlled bearings and connected with a hydraulically controlled actuator for lateral vibration through hydrostatic couplings.

Three rollers are fitted on each shaft, and usually they are fixed at standard gauge (1435 mm) and narrow gauge (1067 mm). When any other gauge is necessary, it can be obtained by adjusting the position of a roller. Thus, gauge-changing work can be carried out easily.

A supporting frame supports a set of rollers-and-shaft assembly, and is installed on the movable bed. The required wheelbase can be obtained by means of moving these beds longitudinally.

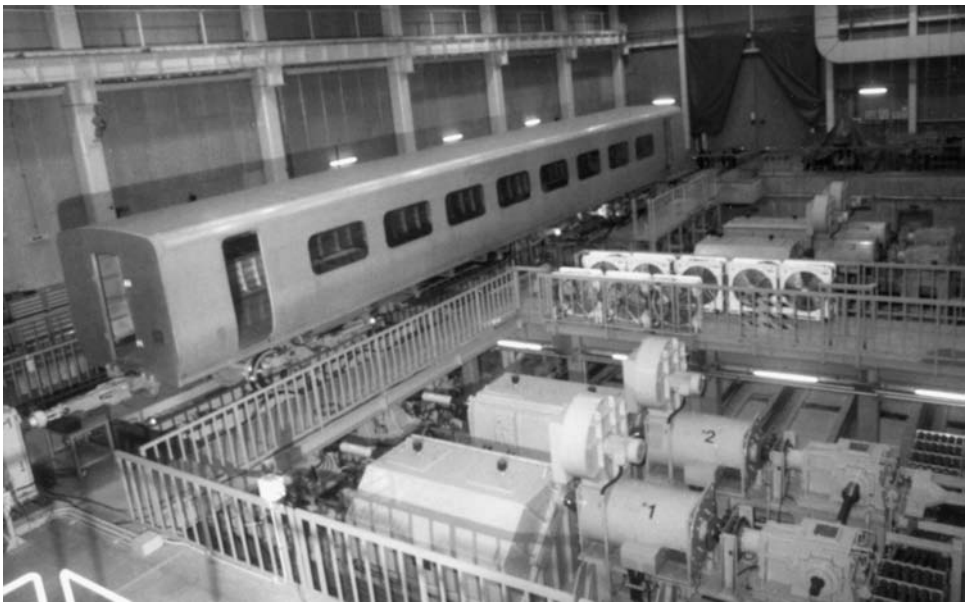

FIGURE 14.15 RTRI rolling stock testing plant.

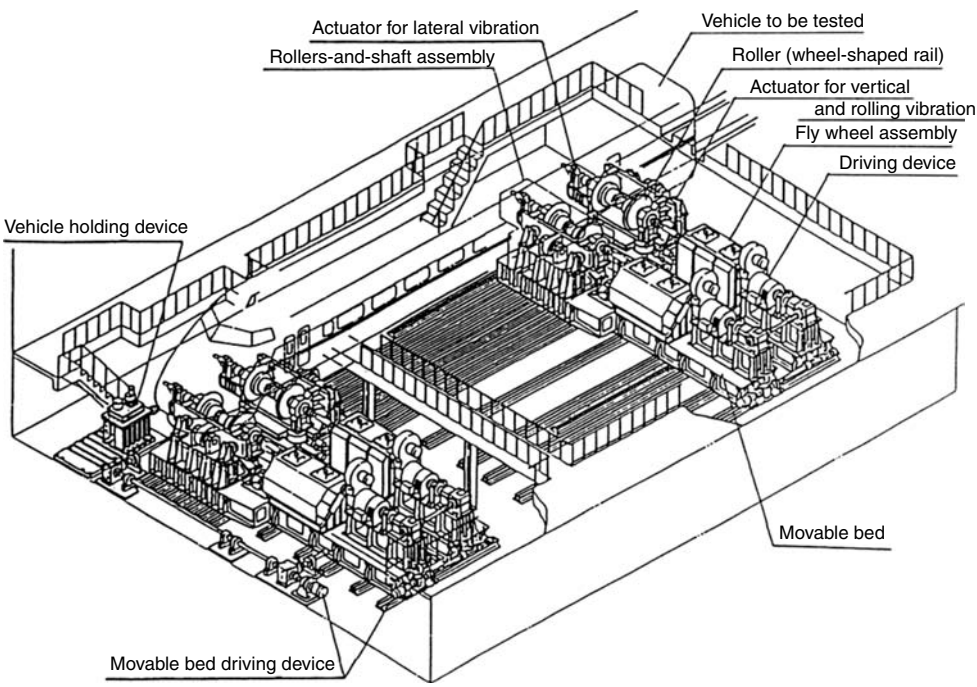

FIGURE 14.16 Sketch of RTRI rolling stock testing plant.

The frame can turn on a movable bed (by up to 10 mrad) and the relative position between the rollers and the test bogie can be finely adjusted by means of a mechanism, "balancing on a ball." A side shaft is provided to avoid a difference in rotations between rollers, thereby achieving synchronous rotation.

2. Flywheel Assembly

The purpose of the flywheel is to absorb or discharge energy corresponding to the inertia of the vehicle being tested. The equivalent mass per axle of the rolling stock mass is given by a flywheel assembly for each roller.

Equivalent mass:
Max. 20 t
Min. 6 t

3. Driving Device

A DC motor of 500 kW is used for each set of rollers-and-shaft assembly, to give the driving device sufficient capacity to absorb the load of the rolling stock. The motor is controlled either in speed or torque mode. The driving shaft is designed to allow the rollers to move laterally.

Driving motor rating: voltage 440 V, current 1250 A, capacity 500 kW

4. Hydraulic Power Source

The hydraulic power source is used for power of the lateral vibration actuators, hydrostatic bearings, and hydrostatic coupling, and consists of pump unit, flow control unit, drain collection unit, oil cooling unit, etc. Lubrication of each gear set and bearing (excepting hydrostatic bearing) is by forced lubrication.

5. Bogie Holding Device

The bogie to be tested is positioned on the rollers by means of the load frame which is connected to the bogie holding device. The load frame is mounted with a mass equivalent to the car body and is designed to withstand the force due to acceleration and deceleration.

6. Building and Foundations

Besides the above-mentioned devices and mechanisms, electric power converter, controlling device, operation and monitoring board, and measurement controlling equipment are installed in the building, which is lined with soundproofing countermeasures.

The foundations, with a mass of 9000 t, is provided under the building so that vibration originating from the mechanical system under test does not transfer to the neighbouring area.

D. The Pueblo Roller Rig (TTC)[1,13]

The roller rig, called the roll dynamics unit (RDU, see Figure 14.17), is a test machine for imparting rotational excitation to the wheels of a rail vehicle. The Rail Dynamics Laboratory, sponsored by the Federal Railroad Administration of the United States Department of Transportation, has been built to provide a powerful test tool for investigating a wide range of rail dynamics problems.

Through a system of drive motors, flywheels, and rollers, the RDU is capable of simulation of both nonpowered vehicles, such as boxcars and passenger cars, and for absorbing power produced

FIGURE 14.17 Roll dynamics unit of TTC.

by self-propelled vehicles, including locomotives and transit cars. The maximum speed is 230 km/h. The unit is composed of modular elements, which can be positioned to match various bogie spacing, axle spacing, and rail equipment gauges.

Each test vehicle wheel rests on and is driven by a supporting roller. Each pair of rollers, mounted on a common shaft, is attached to a drive train, which provides inertia. This interface between the vehicle wheelsets and the roller pair simulates the vehicle travelling over track. The roller allows simulation of vehicles on tangent track having no lateral or vertical irregularities, and also allows simulation of flat curve geometry. Through its flywheels, the RDU is able to simulate resistive forces associated with accelerating of braking of a vehicle.

The RDU enables support and drive of the wheelsets of a four-axle rail vehicle or locomotive bogie. Six- or eight-axle locomotives and cars can be tested with the use of auxiliary support stands. Additionally, the roller rig is equipped with a reaction frame, proving a mounting base for two hydraulic actuators. These actuators are used to apply lateral forces to the side frame of a bogie. The forces can be either steady or vibratory, and can be either push–push or push–pull against the bogie's side frame. This setup provides a very precise, versatile test tool when complemented with high resolution displacement instrumentation. Test conditions are monitored and controlled by the RDU control systems and a pair of computers. The test vehicle responses to the excitation are sensed, processed, and recorded by an acquisition system.

V. OPERATION AND RESULTS

A. Test Methods

The test methods for railway vehicles running on roller rigs differ between testing institutions. The following are test methods used for the Chengdu roller rig and have been formed over many years' testing experience.

1. Status of the Test Vehicle

- In order to ensure the test vehicle is in good running condition, it should run on the roller rig for about 10 h or 500 km before the test starts. During the trial, the running speed should cover the design speed of the vehicle.
- If using a dummy car body instead of a real car body, the mass, moments of inertia, and centre of gravity of the dummy car body should be controlled within an error range of 15% compared with the real car body.

2. Status of the Roller Rig

In order to ensure precision of the test, the following are checked:

- The wear of the rail profile should be less 0.2 mm.
- The roller diameter difference should be less than 0.5 mm for the same roller unit, 1 mm for the bogie, and 2 mm for the vehicle.
- The displacement error of the actuator used on the railway test facility should be less than 5%. The phase error relative to the command signal at 40 Hz should be less than 60°.
- Two longitudinal fixation bars for the middle of the car are positioned in place of the couplers with ball joints, and the length of the bar should be greater than 1 m. One longitudinal fixation bar for the locomotive is positioned in the place of the couplers with ball joints and the length of the bar should be greater than 1.5 m.
- The errors of roller altitude for the same bogie should be less than 2 mm, and for the entire vehicle should be less than 4 mm.

3. Stability Test

Motion stability of a railway vehicle is one of the most important factors of vehicle dynamic behaviour. The main objective of performing a stability test is to identify the vehicle hunting critical speed (see also Chapters 2 and 12). Before introducing the stability test method, we first briefly review the concept of vehicle stability.

A typical limit cycle diagram of wheelset motion is shown in Figure 14.18. In this figure, the solid line indicates a stable limit cycle and the dashed line indicates an unstable limit cycle. When the vehicle speed is lower than V_{C2}, the vehicle system is always stable under any track disturbances. When the vehicle speed is between V_{C2} and V_{C0}, the system equilibrium position is

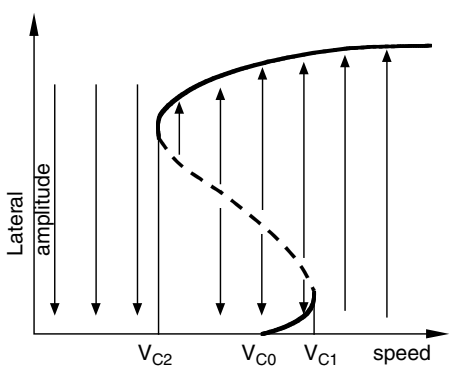

FIGURE 14.18 Limit cycle diagram of wheelset motion: V_{C0}, linear critical speed; V_{C1}, nonlinear critical speed; V_{C2}, nonlinear critical speed.

stable at small track disturbances and unstable at large track disturbances where a limit cycle oscillation will occur. When the vehicle speed is between V_{C0} and V_{C1}, the system equilibrium position is unstable, and small limit cycle oscillations emerge with small track disturbances and large limit cycle oscillations with large track disturbances. Finally, when the vehicle speed is greater than V_{C1}, the system jumps to large limit cycle oscillation at any track disturbance and flange contact may occur. Therefore, V_{C0} which is the Hopf bifurcation point can be defined as the linear critical speed. V_{C1} and V_{C2} can be defined as the nonlinear critical speeds. The nonlinear critical speed V_{C2}, where the first stable limit cycle appears, is normally lower than linear critical speed V_{C0}, thus it should be taken as the speed limit for the vehicle running on tracks.

The object of the stability test is to find out the three speed points V_{C0}, V_{C1}, and V_{C2}. The method of stability testing on the roller rig (for RTU and RVTU) is as follows:

1. Gradually increasing the roller rig speed under pure rolling condition, when a small limit cycle oscillation appears, then the speed V_{C0} is found. Even when the roller rig is in a pure rolling condition, the roller rig always shows small disturbances due to roller (wheel) surface roughness or driving disturbance.
2. Increasing the roller rig speed continuously, when the hunting motion of vehicle system jumps to large amplitude oscillation or even flange contact, then the speed V_{C1} is found.
3. Reducing the speed of the roller rig slowly, when the severe hunting motion reduces to an equilibrium position, then the speed V_{C2} is found.

Since the RVTU is capable of both roller rolling and induced vibrations, it can be used to search the actual critical speed of the vehicle system using actual track irregularity inputs. The actual critical speed is between V_{C2} and V_{C1}, which is related to the track conditions.

In the field line test, the vehicle stability is estimated by the bogie acceleration, which is filtered with a band pass of approximately 0.5 to 10 Hz. If the peak values of acceleration have exceeded 10 m/sec^2 six times consecutively, the vehicle is said to be unstable.

For the stability test, not only should the critical speed be measured, but also the mode shapes of hunting need to be determined. This is achieved by measuring the lateral displacements of car body, bogie frames, and wheelsets.

4. Dynamic Simulation Test

Using the RVTU can simulate the running of the vehicle with track irregularity inputs. Normally, the responses of vehicles, such as accelerations or displacements on car body or bogie, are measured. According to test standards, for instance UIC518, the ride performance is calculated according to the acceleration response in the car body.

Let z_L, y_L, z_R, y_R indicate the irregularity inputs of left and right rails in the time domain for the first roller unit, then the inputs of other roller units are delayed by certain time intervals. The time delays, considering the six-axle vehicle in Figure 14.19 as an example, can be calculated as follows:

$$t1 = l/v \tag{14a}$$

$$t2 = 2l/v \tag{14b}$$

$$t3 = L/v \tag{14c}$$

$$t4 = (L + l)/v \tag{14d}$$

$$t5 = (L + 2l)/v \tag{14e}$$

where l is the bogie wheelbase, L is the distance between bogie centres, and v is the running speed.

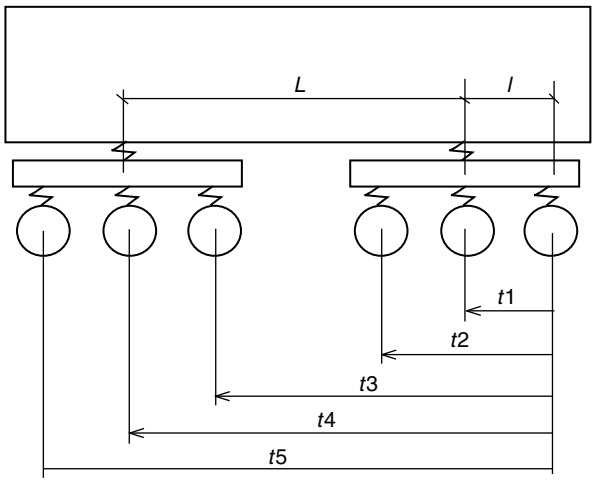

FIGURE 14.19 Time delay of input signals.

In the dynamic test, the measuring items normally include: the accelerations and displacements of car body, bogie frame, and wheelsets (axle box); the relative displacements of primary and secondary suspensions; the relative displacements of motors; the wheel/rail forces; stresses of key parts; temperature of bearing or gear case; etc.

5. Curve Simulation Test

In order to simulate the vehicle curving performance, the roller rig should have the ability to:

- Simulate the curve — set the rollers in a radial position
- Simulate the speeds of inner wheel and outer wheel — to attain different speeds of inner roller and outer roller by using a differential driving system
- Simulate the superelevation and centrifugal force — to set the cant angle of roller unit to simulate the unbalanced centrifugal force caused by superelevation and centrifugal force.

The steps to carrying out a curve simulation test are:

- Set the roller set in a radial position of curve.
- Widen the gauge of roller set according to the curve radius.
- Set up the cant angle of the roller unit according to the unbalanced centrifugal force.
- Lift the test vehicle onto the roller rig and locate it by fixation bars in longitudinal direction. The fixation bars are set at an angle with respect to the car body centreline according to the simulated curve radius.
- The roller rig runs at the prescribed speed.
- Adjust the speed difference of inner and outer rollers according to the curve radius and running speed.
- For steady-state simulation, the roller rig is in a rolling only condition and the wheel–rail interaction forces can be measured.
- For dynamic simulation, the track irregularity inputs are considered. The wheel–rail interaction forces and the responses such as acceleration, displacement of car body, bogie frame, and wheelset can be measured.
- Then the derailment ratio Q/P, lateral force H, wheel load reduction rate $\Delta P/P$, and ride index W can be obtained.

6. Power Test

The aim of the power test is to evaluate the driving or braking behaviour of the motor car. The power test is performed mainly at the Naples roller rig. A few examples of power tests performed in the Naples roller rig are described in Section IV.C.2.

7. Modal Analysis Test

When the car body, bogie frame, and wheelset are considered as rigid bodies and are suspended by primary and secondary suspensions, the vehicle is a typical multibody system. Thus the natural vibrations of the vehicle system will appear at some frequencies. By using the RVTU or VTU, the vibration modes (self-vibration frequency and modal shape) can be determined.

To perform the modal analysis test, the lateral, vertical, roll, pitch and yaw motions are normally considered. The rollers (or movable short rails) should be excited in separate modes. A swept sine wave or white noise is used as the roller rig inputs. Through analysing the responses of car body and bogie frames, the resonance points under each mode will be determined and the modal frequencies can be obtained.

8. Storage Security Test

Loading methods are very important for some special goods, such as columned goods (pipes, cans, wood), destructible goods (glass, apparatus) and explosive goods (nuclear material, detonators). The use of RVTU or VTU can validate the goods behaviour, such as:

- The security of loading under vibration, impact, and lateral force (superelevation, centrifugal force)
- The stability of goods after long-distance travel
- The behaviour of a new loading method
- The dynamic environment of goods during transportation, such as vibration acceleration, temperature, pressure, and force.

A roller rig has great flexibility and can perform diverse tasks such as estimation of creep forces, wear of wheel and rail profiles, adhesion between wheel and rail, natural frequency and mode, response control, etc.[12–23]

B. Differences between Roller and Track

1. Differences of Geometry Relationship

a. Calculation Method of Wheel–Roller Geometry Relationship

In theoretical analysis of railway vehicle dynamics, the first step is the determination of the wheel–rail geometry relationship.[24,25] The main difference between a vehicle running on track and on a roller rig is the wheel–rail contact and wheel–roller contact. In order to understand the behaviour of a vehicle running on a roller rig, a numerical method for wheel–rail geometry calculation called the "line tracing method" will be introduced below.[26]

Owing to the symmetry of the wheelset structure a half wheelset model is considered. The analysis model is shown in Figure 14.20. $OXYZ$ is the absolute coordinate axis for the roller, $G''wX''Y''Z''$ is the wheelset coordinates, and $G''wX'Y'Z$ is the wheelset fixed coordinate. φ and θ are the yaw angle and roll angle with respect to $G''wX''Y''Z''$. Term Y''_{Gw} is the lateral displacement of wheelset. According to directional cosine principle, the axis line $G''wY'$ in wheelset coordinate

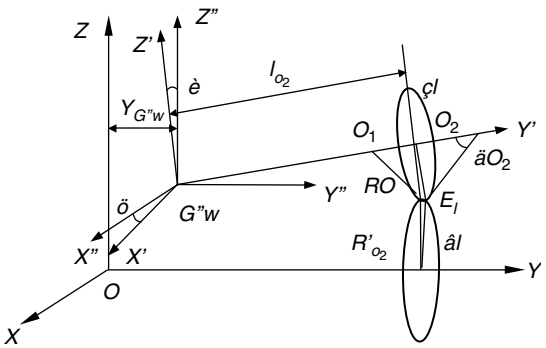

FIGURE 14.20 Model of wheel–roller geometry relationship.

$G''wX''Y''Z''$ can be described as:

$$L_x = -\cos\theta\sin\varphi; \qquad L_y = \cos\theta\cos\varphi; \qquad L_z = \sin\theta$$

In the figure, E_l is the contact point, δ_{O_2} is the contact angle, η_l is the contact circle on wheel, O_2 is the centre of the contact circle, R_{O_2} is the radius of the contact circle, l_{O_2} is the distance from the contact circle to the centre of the wheelset. The normal line from contact point E_l intersects the wheelset axis line $G''wY'$ at point O_1. Then, the distance from O_1 to O_2 is:

$$O_1O_2 = H = R_{O_2} tg\delta_{O_2} \tag{14.1}$$

The distance from O_1 to E_l is

$$O_1E_l = \frac{R_{O_2}}{\cos\delta_{O_2}} \tag{14.2}$$

The coordinates of O_1 and O_2 in the axis system $G''wX''Y''Z''$ are

$$\begin{aligned} X_{O_2} &= l_{O_2}L_x \\ Y_{O_2} &= l_{O_2}L_y \\ Z_{O_2} &= l_{O_2}L_z \end{aligned} \tag{14.3}$$

$$\begin{aligned} X_{O_1} &= (l_{O_2} - H)L_x \\ Y_{O_1} &= (l_{O_2} - H)L_y \\ Z_{O_1} &= (l_{O_2} - H)L_z \end{aligned} \tag{14.4}$$

The equation of the contact circle in $G''wX''Y''Z''$ is

$$\begin{aligned} &L_x(X - X_{O_2}) + L_y(Y - Y_{O_2}) + L_z(Z - Z_{O_2}) = 0 \\ &(X - X_{O_2})^2 + (Y - Y_{O_2})^2 + (Z - Z_{O_2})^2 = R_{O_2}^2 \end{aligned} \tag{14.5}$$

The equation of the plane, which is perpendicular to $G''wX''Z''$, passes O_1, and has an angle β_l with respect to axis Z'', is

$$Z = -ctg\beta_l X + C \qquad (C \text{ is a constant}) \tag{14.6}$$

Considering the coordinates of point O_1, Equation 14.6 becomes

$$X = -tg\beta_l Z + (l_{O_2} - H)(L_z tg\beta_l + L_x) = -tg\beta_l Z + K \tag{14.7}$$

where $K = (l_{O_2} - H)(L_z tg\beta_l + L_x)$.

Inserting Equation 14.7 into the first formula of Equation 14.5, we get

$$Y = \frac{L_x tg\beta_l - L_z}{L_y} Z + \frac{L_x(X_{O_2} - K) + L_y Y_{O_2} + L_z Z_{O_2}}{L_y}$$

if

$$K_1 = \frac{L_x tg\beta_l - L_z}{L_y} \qquad \text{and} \quad K_2 = \frac{L_x(X_{O_2} - K) + L_y Y_{O_2} + L_z Z_{O_2}}{L_y}$$

we have

$$Y = K_1 Z + K_2 \tag{14.8}$$

Inserting Equation 14.8 into the second formula of Equation 14.5, we get

$$AZ^2 + BZ + C = 0 \tag{14.9}$$

where $A = tg\beta_l + K_1^2 + 1$

$$B = 2(-tg\beta_l K + X_{O_2} tg\beta_l - Y_{O_2} K_1 - Z_{O_2} + K_1 K_2)$$

$$C = (K - X_{O_2})^2 + (K_{O_2} - Y_{O_2})^2 + Z_{O_2}^2 - R_{O_2}^2$$

From Equation 14.9, Z can be derived as

$$Z = \frac{-B - \sqrt{B^2 - 4AC}}{2A} \tag{14.10}$$

Here, the location of contact point E_l is determined according to Equation 14.7, Equation 14.8, and Equation 14.10. However, in those equations, there is an unknown variable β_l (for wheel–rail case, $\beta_l = 0$). It is necessary to add another equation. Generally, the wheelset centre is assumed to be in the same vertical plane of roller. Thus, there is a relation:

$$X + R'_{O_2} \sin \beta_l = 0 \tag{14.11}$$

When l_{O_2} changes, the other values such as R_{O_2}, R'_{O_2}, and δ_{O_2} will also be changed, and the coordinates of possible contact points E_l, X_{E_l}, Y_{E_l}, Z_{E_l}, and β_l can be obtained. A series of possible contact points form a line called the "tracing line." The contact point E_l must be on the tracing line. Considering the right side of the wheelset and adjusting the roll angle θ, the contact points E_l and E_r can be determined under the condition of ensuring that the left and right wheel keep contact with the rollers. Furthermore, the radius of contact circle $R_{l,r}$, contact angle $\delta_{l,r}$ and the distance of contact circle to the centre of wheelset $l_{l,r}$ can be decided. The difference of radius of contact circle ΔR,

difference of contact angle $\Delta\delta$, equivalent conicity λ_e, contact angle parameter ε_e, wheelset gravitational stiffness $K_{sy,}$ and gravitational angular stiffness $K_{s\varphi}$ can be calculated as:

$$\Delta R = R_l - R_r; \qquad \lambda_e = \frac{\Delta R}{2Y_{G''w}}$$

$$\Delta\delta = \delta_l - \delta_r; \qquad \varepsilon_e = \frac{\Delta\delta}{2Y_{G''w}}(l_l - l_r)$$

$$K_{sy} = \frac{-\sin\delta_l(Z_{E_r}\sin\delta_r - Y_{E_r}\cos\beta_r\cos\delta_r) + \sin\delta_r(Z_{E_l}\sin\delta_l + Y_{E_l}\cos\beta_l\cos\delta_l)}{Y_{G''w}D}$$

$$K_{s\varphi} = \frac{(-X_{E_r}\sin\delta_l + Y_{E_l}\sin\beta_l\cos\delta_l)(Z_{E_r}\sin\delta_r - Y_{E_r}\cos\beta_r\cos\delta_r)}{\varphi D} + \frac{(X_{E_l}\sin\delta_r - Y_{E_r}\sin\beta_r\cos\delta_r)(Z_{E_l}\sin > \delta_l + Y_{E_l}\cos\beta_l\cos\delta_l)}{\varphi D}$$

where

$$D = \cos\beta_l\cos\delta_l(Z_{E_r}\sin\delta_r + Y_{E_l}\cos\beta_r\cos\delta_r) + \cos\beta_r\cos\delta_r(Z_{E_l}\sin\delta_l - Y_{E_r}\cos\beta_l\cos\delta_l)$$

b. Geometry Difference of Wheel–Rail Contact and Wheel–Roller Contact

A roller rig uses a limited radius roller instead of straight track. When the yaw angle φ of the wheelset is zero, the geometry relationship of wheel–roller contact is the same as wheel–rail contact. If the yaw angle is not zero, a difference of geometry exists. The following parameters for wheel, rail, and roller are considered:

Track gauge is 1435 mm, wheel diameter is 915 mm, roller diameter is 1370 mm, rail cant is 1/40, type of wheel profile is LM (a Chinese worn-type wheel profile), type of rail profile (roller) is 60 kg (similar to UIC S1002 profile).

For analysing the difference between wheel–rail contact geometry and wheel–roller contact geometry, yaw angle φ is chosen as 3°. First, for wheel–rail contact, the normal line of contact point is always in the vertical plane, which means the angle β is zero. However, for wheel–roller contact, there is an angle between the normal line and vertical plane. Figure 14.21 shows the angle of left wheel contact point β_l at different lateral displacements of the wheelset. When the yaw angle is 3°, the angle β is about 0.038 rad ($\approx$2.2°). When the lateral displacement of the wheelset reaches 10 mm, a change of the angle β_l occurs and the value of β_l becomes negative, resulting in flange contact.

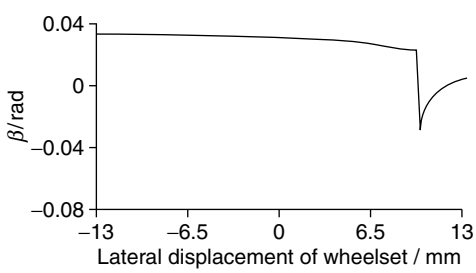

FIGURE 14.21 Angle β_l.

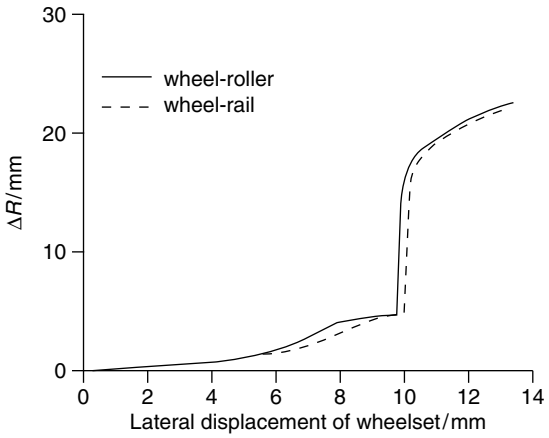

FIGURE 14.22 Comparison of ΔR.

Figure 14.22 illustrates the comparison of the difference in radius of the contact circle ΔR. When the lateral displacement is less than 5 mm, there is almost no difference in ΔR. Once the lateral displacement is larger than 5 mm, the difference in radius of contact circle ΔR for wheel–roller contact is larger than wheel–rail contact. At approximately 10 mm flange contact occurs and the value of ΔR increases rapidly. The flange contact for wheel–roller contact appears earlier than wheel–rail contact. The situation for the difference in contact angle $\Delta\delta$ is similar to the case of ΔR. After flange contact, the difference in contact angle $\Delta\delta$ of wheel–roller contact is smaller than wheel–rail contact, which is shown in Figure 14.23. Since the equivalent conicity λ_e is derived from ΔR, results are similar, as shown in Figure 14.24. Figure 14.25 shows the comparison of roll angle θ. It can be seen that the roll angle θ in wheel–roller is larger than in the case of wheel–rail.

Comparing the wheelset gravitational stiffness K_{sy} and gravitational angular stiffness $K_{s\varphi}$, it is found that the stiffness K_{sy} is nearly the same for wheel–rail contact and wheel–roller contact, but there is a big difference for angular stiffness $K_{s\varphi}$. At 3° of wheelset yaw angle, $K_{s\varphi}$ for wheel–rail contact is nearly zero before the flange contact, but for wheel–roller contact, $K_{s\varphi}$ is negative before flange contact (see Figure 14.26). Therefore, the vehicle running on the roller rig is less stable due to the negative value of $K_{s\varphi}$.

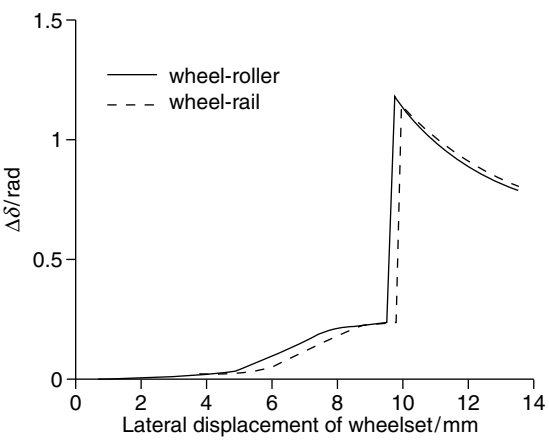

FIGURE 14.23 Comparison of $\Delta\delta$.

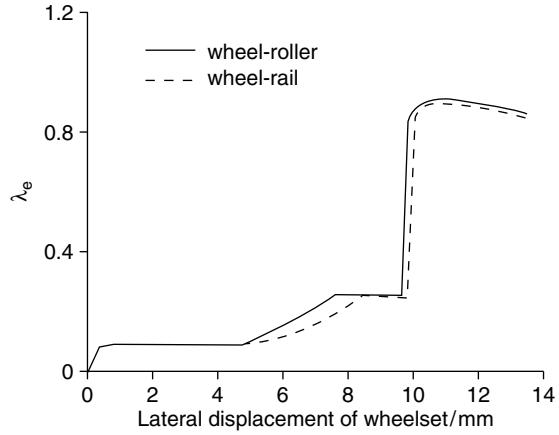

FIGURE 14.24 Comparison of λ_e.

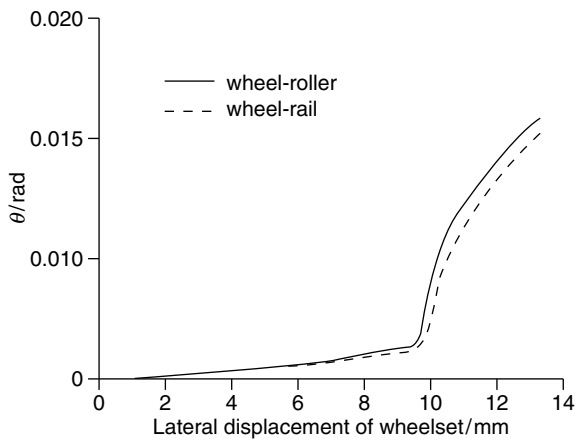

FIGURE 14.25 Comparison of θ.

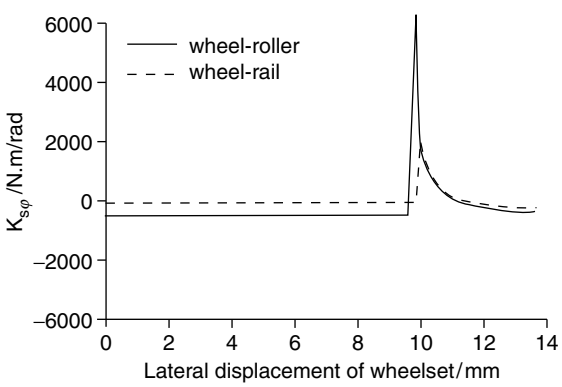

FIGURE 14.26 Comparison of $K_{s\varphi}$.

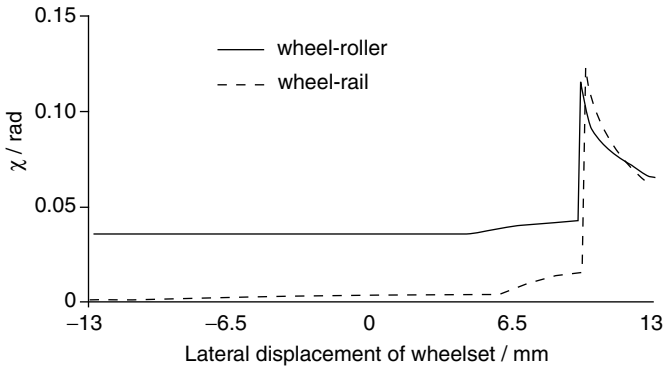

FIGURE 14.27 Comparison of χ.

The contact point is not at the bottom of the contact cycle, and there is a leading angle χ shown in Figure 14.27. It is apparent that the leading angle χ for wheel–roller contact is larger than the value in the case of wheel–rail contact. This is the reason why the absolute value of gravitational angular stiffness $K_{s\varphi}$ for wheel–roller contact is larger than for wheel–rail contact.

2. Difference in Creep Coefficient

The creep forces are calculated by the following formula

$$T_1 = -f_{11}\gamma_1, \qquad T_2 = -f_{22}\gamma_2 - f_{23}\omega_3, \qquad M_3 = f_{23}\gamma_2 - f_{33}\omega_3 \tag{14.12}$$

where T_1, T_2, and M_3 are longitudinal creep force, lateral creep force, and spin creep moment. γ_1, γ_2, and ω_3 are the longitudinal, lateral, and spin creepages, which are related to the movement of wheel and rail (roller). f_{11}, f_{22}, f_{23}, and f_{33} are the creep coefficients, which are defined as:

$$f_{11} = E(ab)c_{11}; \quad f_{22} = E(ab)c_{22}; \quad f_{23} = -f_{32} = E(ab)^{3/2}c_{23}; \quad f_{33} = E(ab)^2 c_{22} \tag{14.13}$$

where E is the modulus of rigidity. a and b are the length of the semiaxis of the contact ellipse in the rolling and lateral directions. C_{ij} are the Kalker's creepage and spin coefficients, which depend only on Poisson's ratio σ and the ratio of the semiaxes of the contact ellipse. Thus, the creep coefficients are significantly affected by the contact ellipse dimensions (see also Chapter 4, Section III E).

According to Hertz's static solution, the semiaxis of the contact ellipse a and b can be expressed as:

$$\left(\frac{a}{m}\right)^3 = \left(\frac{b}{n}\right)^3 = \frac{3N(1-\sigma)^2\rho}{2\pi E} \tag{14.14}$$

where N is the normal force. m and n are coefficients which can be found by using Hertz's table. ρ is the characteristic length which can be described as:

$$\frac{1}{\rho} = \frac{1}{R_1} + \frac{1}{R_1'} + \frac{1}{R_2} + \frac{1}{R_2'} \tag{14.15}$$

where R_1 and R_1' are the principal radii of wheel profile. R_2 and R_2' are the principal radii of rail or roller profile. For wheel–rail contact, $R_2 = \infty$. Thus it is obvious that characteristic length ρ for wheel–rail contact is larger than the case for wheel–roller contact. For example, principal radii of

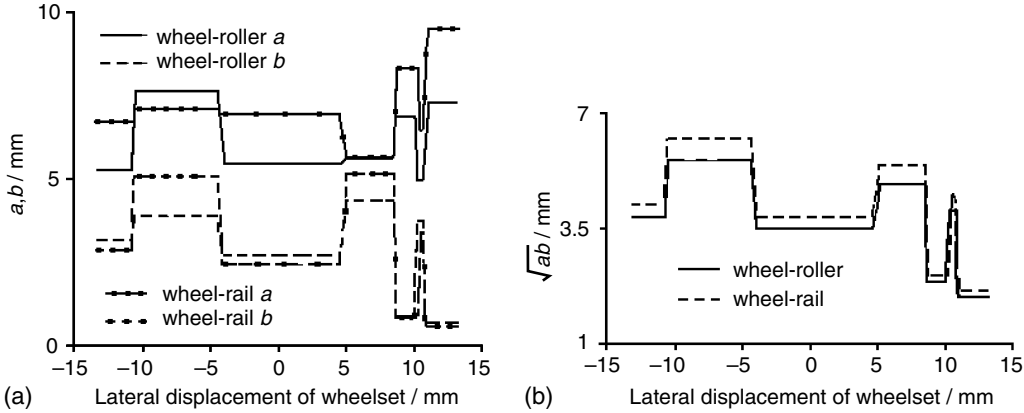

FIGURE 14.28 Comparison of contact ellipses: (a) semiaxes of the contact ellipse; (b) area of the contact ellipse.

wheel profile $R_1 = 475.5$ mm and $R_1' = 500$ mm, the principal radii of roller profile $R_2 = 685$ mm (∞ for rail) and $R_2' = 300$ mm, the characteristic length ρ for wheel–rail contact is 134.0 mm, and for the wheel–roller contact is 112.4 mm; the difference is about 20%. Under the condition of an axle load of 11,400 kg, the semiaxes of the contact ellipse a and b for wheel–rail and wheel–roller contact is shown in Figure 14.28a. Since the profiles of wheel and rail are composed of different curves and lines, the calculated a and b are not constants.

When the wheelset lateral displacement is zero, the semiaxis a for wheel–roller contact is shorter than the value for wheel–rail contact. The reason is that the radius of the roller is less than the radius of the rail, while the semiaxis b for wheel–roller contact is little larger than the value for wheel–rail contact. This situation is easily explained, since the axle load for the two cases is the same, when the semiaxis a becomes smaller, the semiaxis b will become larger in order to support the same wheel load. When the wheelset is at its central position, the area of contact ellipse $\sqrt{ab}$ for wheel–roller contact is smaller than for wheel–rail contact (see Figure 14.28b). According to Equation 14.13, the area of the contact ellipse directly affects the creep coefficients, so it can be estimated that the creep coefficients for wheel–roller contact should be smaller than the values for wheel–rail contact. Figure 14.29 shows the comparison of the creep coefficients f_{11} and f_{33}.

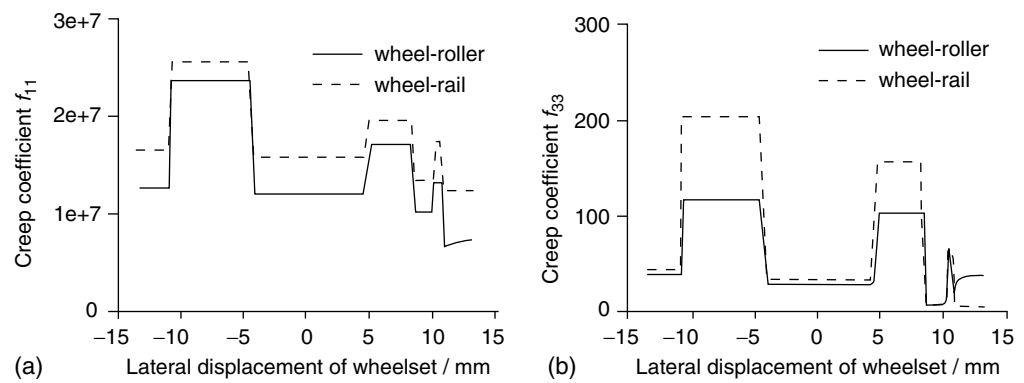

FIGURE 14.29 Comparison of creep coefficients: (a) creep coefficient f_{11}; (b) creep coefficient f_{33}.

The value of f_{11} for wheel–roller contact is 20% less than for wheel–rail contact. For f_{33}, the maximum difference is about 40%.

3. Differences in Stability

There are two main reasons for the difference between wheel–rail contact and wheel–roller contact. The first is that the creep coefficients for wheel–roller contact are smaller than the values for wheel–rail contact, and the second is that the wheelset gravitational angular stiffness $K_{s\varphi}$ is negative for wheel–roller contact when the yaw angle φ is not zero. In order to discuss the difference of vehicle stability on a roller rig, the equations of motion of a single wheelset with primary suspension are considered,[27,28]

$$\begin{aligned} &M_w\ddot{y}_w + \frac{2f_{22}}{v}\dot{y}_w + \left(K_{py} - \frac{2f_{23}\varepsilon}{R_0 b} + \frac{W\varepsilon}{b}\right)y_w + \frac{2f_{23}}{v}\dot{\varphi}_w - 2f_{22}\varphi_w = 0 \\ &I_{wz}\ddot{\varphi}_w - \frac{2f_{23}}{v}\dot{y}_w + \left(\frac{2f_{11}\lambda_e b}{R_0} - 2f_{33}\frac{\varepsilon}{R_0 b}\right)y_w + \left(\frac{2f_{11}b^2}{v} + 2f_{33}\right)\dot{\varphi}_w \\ &\quad + (K_{px}b_1^2 + K_{s\phi} + 2f_{23})\varphi_w = 0 \end{aligned} \tag{14.16}$$

where y_w and φ_w are the lateral displacement and yaw angle of wheelset. M_w and I_{wz} are the mass and moment of inertia around axis z. K_{px} and K_{py} are the suspension stiffness in the rolling direction and the lateral direction. R_0 is the wheel contact radius. b is the half distance between contact points. b_1 is the half distance between primary suspension. W is the axle load. v is the forward speed.

Through variable transformation, Equation 14.16 can be presented as

$$\dot{Y} = AY \tag{14.17}$$

The condition of nonzero solution is that the following form is satisfied

$$|\lambda I - A| = 0 \tag{14.18}$$

Expanding Equation 14.18, it can be written as

$$a_0\lambda^4 + a_1\lambda^3 + a_2\lambda^2 + a_3\lambda + a_4 = 0 \tag{14.19}$$

According to the Hurwitz law of stability, the following condition should be satisfied if the wheelset is stable

$$\Delta_1 = a_1 > 0$$

$$\Delta_2 = \begin{vmatrix} a_1 & a_3 \\ a_0 & a_2 \end{vmatrix} > 0$$

$$\Delta_3 = \begin{vmatrix} a_1 & a_3 & a_0 \\ a_0 & a_2 & a_4 \\ 0 & a_1 & a_3 \end{vmatrix} > 0$$

$$\Delta_4 = a_4\Delta_3 > 0$$

Since Equation 14.16 can ensure that the coefficient a_i in Equation 14.19 is positive, then Δ_1 and Δ_2 are larger than zero, so only Δ_3 needs to be considered. When $\Delta_3 = 0$, the critical

speed V_c can be presented as:

$$V_c^2 = \frac{\left[2f_{11}b^2\left(K_{py} + \frac{W\varepsilon}{b}\right) + 2f_{22}(K_{px}b^2 + K_{s\varphi})\right](2f_{22}I_{wz} + 2f_{11}b^2M_w)}{\frac{\lambda_e}{R_0 b}(2f_{22}I_{wz} + 2f_{11}b^2M_w)^2 - \left[M_w(K_{px}b_1^2 + K_{s\varphi}) - I_{wz}\left(K_{py} + \frac{W\varepsilon}{b}\right)\right]^2} \tag{14.20}$$

As discussed, considering a wheelset on a roller rig, the gravitational angular stiffness $K_{s\varphi}$ has a negative value and this will result in the numerator decreasing and the denominator increasing. Thus, the critical speed V_c reduces. This result has been described in other papers.[29–33]

Figure 14.30 shows a Chinese high-speed passenger car with TB wheel profile (a conical profile). The hunting stability of the vehicle on roller rig and on rail are compared. Figure 14.31 is the limit cycle of the vehicle on a roller rig and on rail. It can be seen that the critical speed of the vehicle on the roller rig is less than the critical speed on rail. The speed difference is approximately 40 to 60 km/h. As would be expected, the speed difference between a vehicle on a roller rig and on rail is not the same for different vehicles or different parameters. Figure 14.32 shows the influence of the longitudinal stiffness primary suspension (it is 24 MN/m in Figure 14.31). It is seen that the speed difference between a vehicle on a roller rig and on rail becomes larger with an increase in the longitudinal stiffness. Therefore, it is necessary to modify the critical speed of the vehicle being tested on the roller rig by theoretical analysis or by a test method. Using a test method to modify the critical speed has been adopted on the Munich roller rig[6] by changing the states of the rollers, such as widening the gauge, or tilting the rollers, according to the requirement of equivalent conicity.

FIGURE 14.30 Passenger car on the roller rig.

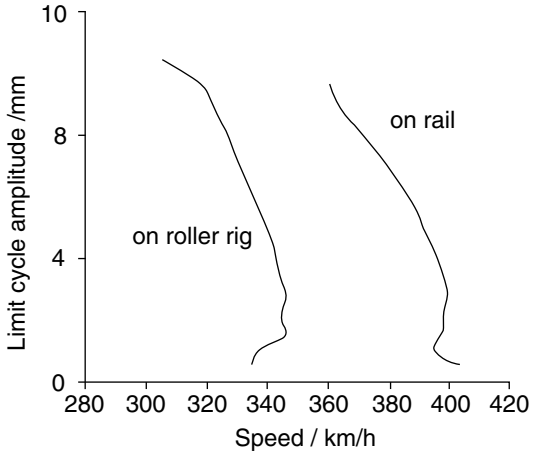

FIGURE 14.31 Comparison of critical speed.

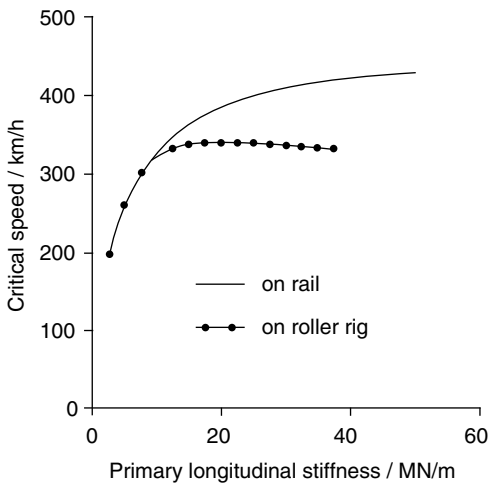

FIGURE 14.32 Influence of stiffness.

4. Difference in Vibration Response

Dynamic tests include not only stability tests but also the dynamic response test, which is performed to investigate the vibration response of a car body subject to track irregularity inputs. Rig results can be compared with line tests, and the difference in vibration response for the vehicle tested on the RVTU should be clear.

Inclusion of track irregularity inputs in the equations of motion of the wheelset gives:

$$M_w\ddot{y}_w + \frac{2f_{22}}{v}\dot{y}_w + \left(K_{py} - \frac{2f_{23}\varepsilon}{R_0 b} + \frac{W\varepsilon}{b}\right)y_w + \frac{2f_{23}}{v}\dot{\varphi}_w - 2f_{22}\varphi_w = f_{22}\left(\frac{\dot{y}_{\mathrm{tl}}}{v} + \frac{\dot{y}_{\mathrm{tr}}}{v}\right) \quad (14.21)$$

$$I_{wz}\ddot{\varphi}_w - \frac{2f_{23}}{v}\dot{y}_w + \left(\frac{2f_{11}\lambda_e b}{R_0} - 2f_{33}\frac{\varepsilon}{R_0 b}\right)y_w + \left(\frac{2f_{11}b^2}{v} + 2f_{33}\right)\dot{\varphi}_w + (K_{px}b_1^2 + K_{s\phi} + 2f_{23})\varphi_w$$

$$= \frac{f_{33}}{v}(\dot{\phi}_{tl} + \dot{\phi}_{tr})$$

where $\dot{y}_{tl}$ and $\dot{y}_{tr}$ are the lateral velocities of the left and right tracks. $\dot{\phi}_{tl}$ and $\dot{\phi}_{tr}$ are the yaw angular velocities of the left and right rails. Owing to the reduction in creep coefficients f_{ii} and the gravitational angular stiffness $K_{s\varphi}$, the damping and stiffness values for the variable φ_w are reduced, and therefore the vibration response of a vehicle on a roller rig will be larger than the case of running on rail.

By taking a Chinese high-speed passenger car as an example, shown in Figure 14.30, the comparison for the responses on roller rig and on rail is made. Figure 14.33 shows the acceleration response in the frequency domain. When the frequency is larger than 6 Hz, the acceleration response is nearly the same between roller rig and rail but at a low frequency the acceleration response of vehicle on roller is larger than the case on rail.

The example has been also analysed by using the code MEDYNA.[4] The following power spectral density of track irregularity is used:

$$S_{yy}(\omega) = S_{zz}(\omega) = \frac{0.1078 \times 105}{1 + 0.6804 \times \omega^2 + 0.2886 \times 10^{-3} \times \omega^4} \tag{14.22}$$

The sampling point is at floor height above the bogie, with 1 m offset from the centre. The ISO2631 standard is used to evaluate the difference in acceleration response. Comparison of the results is shown in Table 14.4. Data above the line in the row is for lateral and data below is for

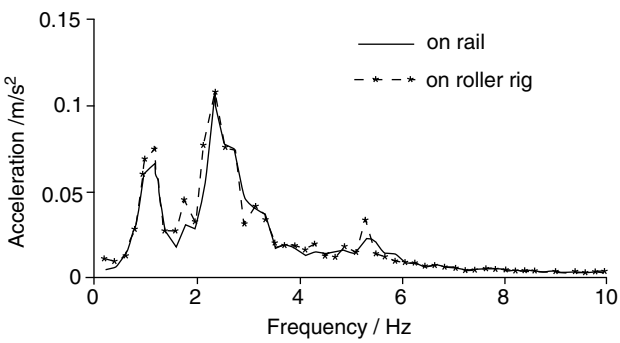

FIGURE 14.33 Comparison of acceleration response.

TABLE 14.4
Comparison of Acceleration Response

Speed/km/h	120	160	220	320	400
On rail	0.3045 / 0.1504	0.4162 / 0.2586	0.4769 / 0.3646	0.5615 / 0.5317	0.7027 / 0.6221
On roller rig	0.3053 / 0.1540	0.4230 / 0.2650	0.4910 / 0.3835	0.5970 / 0.6160	0.6896 / 0.7788

vertical. It is obvious that the results for a vehicle on a roller rig are larger than the results on rail, whether for lateral or vertical.

5. Difference in Curve Simulation

Curve simulation is difficult to imitate on a roller rig, especially for a vehicle passing through a transition curve. Owing to this, curve simulations are limited to circular curves. The cant of the roller unit is used to simulate the unbalanced centrifugal force caused by superelevation and centrifugal force. The cant angle of the roller unit can be expressed as:

$$\theta_d = \frac{v^2}{gR} - \frac{h}{2d} \tag{14.23}$$

where v is speed, R is the radius of curvature, h is the superelevation, and $2d$ is the gauge.

In order to show the differences in curve simulation, an example with a curve radius of $R = 300$ m and superelevation $h = 90$ mm is presented in Figure 14.34. A passenger vehicle modeled using the SIMPACK vehicle dynamics code was used in this example. The results shown in Figure 14.34 indicate that the lateral displacement of wheelset, lateral wheel–rail force Q, derailment factor Q/P, wheel load reduction ratio $\Delta P/P$ on a roller rig are a little smaller than the values on rail. The difference is less than 10%, showing that curve simulation on a roller rig can basically show the characteristics of vehicles passing through a circular curve.

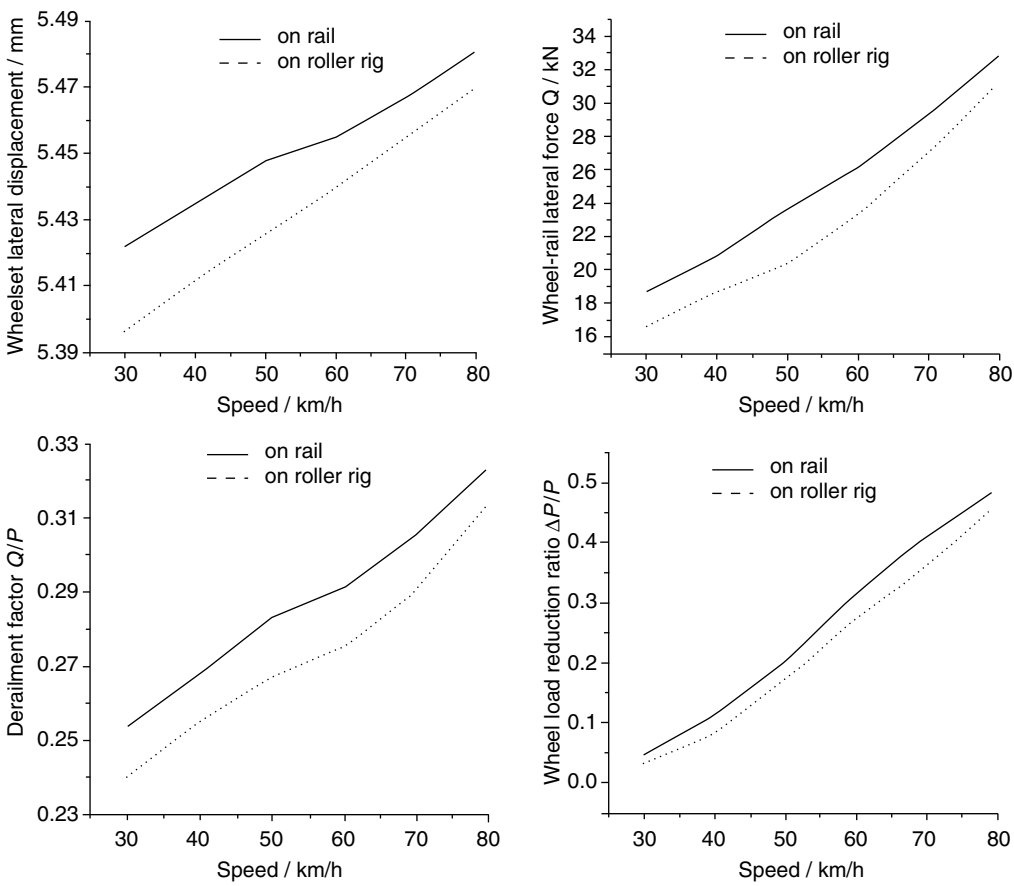

FIGURE 14.34 Comparison of curve simulation.

C. Influence of Setup Errors on Roller Rig Vehicle Stability

The roller rig should have the ability to evaluate accurately the dynamic behaviour of the vehicle system but various setup errors always exist on a roller rig due to wear, incorrect installation, and different environmental (friction) conditions. The following shows the influence of various setup errors of a roller rig on vehicle stability using the example of a Chinese high-speed passenger car (shown in Figure 14.30) with a TB wheel profile.[4,34]

1. Diameter of the Rollers

Wear and machining errors on the roller surface are practically unavoidable. The nominal diameter of the rollers in Chengdu is 1370 mm, with an allowable minimum diameter of 1300 mm. A smaller roller radius will cause larger negative gravitational angular stiffness $K_{s\varphi}$, which may cause hunting critical speed to become lower. Figure 14.35 shows the limit cycle of the passenger car on the roller with diameters of 1370 and 1300 mm. It is seen that the smaller the roller diameter, the lower the critical speed.

2. Gauge of the Rollers

For an RTU, the gauge of the rollers is fixed during the test but after adjusting the rollers to meet a different gauge, an error in the gauge may occur. For an RVTU, the gauge can be changed arbitrarily. Theoretical results indicate that the influence of gauge is small when using a TB wheel profile but when using the LM worn-type wheel profile the influence of gauge on critical speed is greater, as seen in the results of Figure 14.36. When the gauge is widened, the critical speed increases, which is one of the methodologies used on the Munich roller rig to match test results to line measurements.

3. Cant of the Rollers

In the early era of railways the cant of the rail was zero, later it became 1/20 and currently the normal cant is 1/40. The influence of different cant is shown in Figure 14.37. It is evident that when the roller is without cant, the critical speed is at its lowest, with increase in cant, the critical speed increases, but within the range of 1/40 to 1/10 the influence is relatively small.

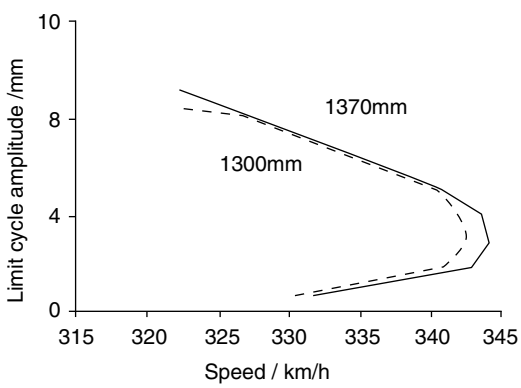

FIGURE 14.35 Influence of diameter of roller.

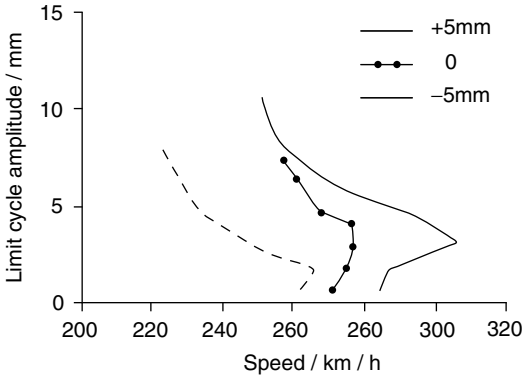

FIGURE 14.36 Influence of gauge.

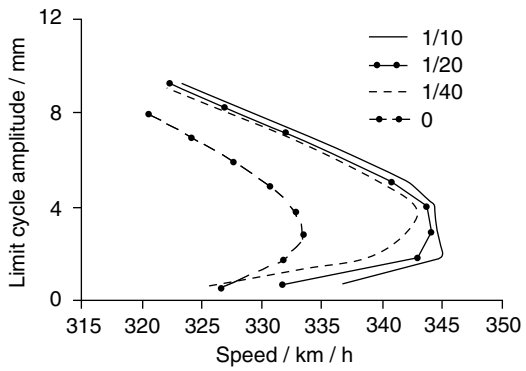

FIGURE 14.37 Influence of cant of roller.

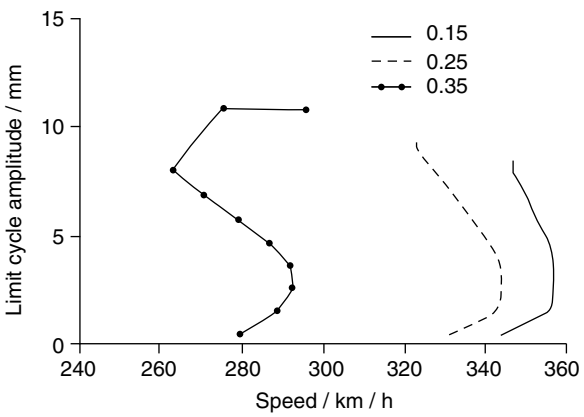

FIGURE 14.38 Influence of friction coefficient.

4. Coefficient of Friction on the Contact Surface

A wheel rolling on rollers makes the contact surface smooth and contamination makes the friction characteristic change. The influence of friction coefficient on stability is shown in Figure 14.38. It is seen that the lower the friction coefficient, the higher the critical speed.

5. Vehicle Position on the Roller Rig

During the test the vehicle sits on top of the rollers and is fixed in the longitudinal direction. Since errors exist in the wheelbase, bogie centre distance, and position of roller unit, it is difficult to position accurately the wheels on top of the rollers (see Figure 14.39). Such errors will influence the critical speed, as shown in Figure 14.40. When all the wheels of the vehicle are forward of the centreline of the rollers by 10 mm, the critical speed reduces, contrarily when all wheels are rearward by 10 mm, the critical speed is increased. Such interesting results are validated by the stability tests.

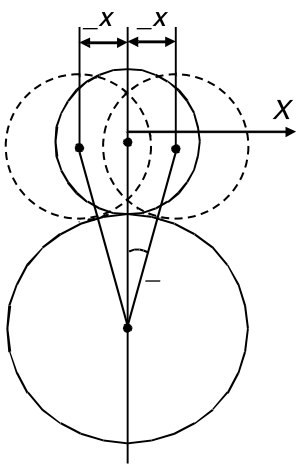

FIGURE 14.39 Wheel position.

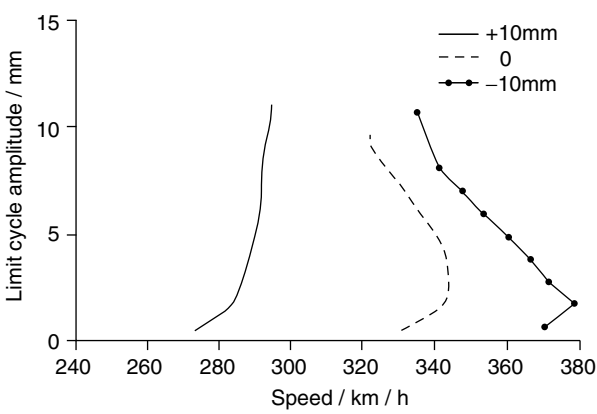

FIGURE 14.40 Influence of friction coefficient.

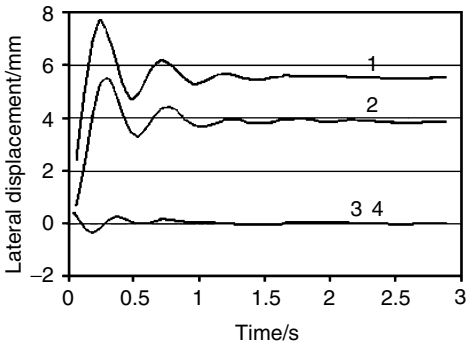

(a) wheelset 1 is with yaw angle

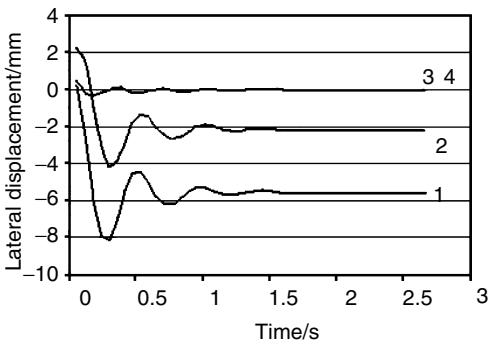

(b) wheelset 2 is with yaw angle

FIGURE 14.41 Influence of wheelset yaw angle.

6. Yaw Angle between Wheelset and Roller Axle

The wheels of the test vehicle should stay on top of the rollers and be parallel with the roller axle. However, the wheelsets within a bogie are difficult to keep parallel with each other. There is a yaw angle between the wheelset and roller axles which results in the wheelset moving to one side of roller unit or even into flange contact. Figure 14.41 shows the simulation results of vehicle motion due to a wheelset yaw angle. It is known that when wheelset one is set a yaw angle, it moves from the central position, which in turn causes wheelset two to move from the central position. When wheelset two is set to a yaw angle, again, both wheelsets one and two leave the central position. Thus if one wheelset has a yaw angle with respect to roller axle, it will cause the bogie to go to one side. Normally, this yaw misalignment of the wheelsets cannot be adjusted during the test. In order to allow the wheelset to align centrally on the roller unit, it is necessary to adjust the yaw angle of the roller axle to match the wheelset yaw angle.

It should be stated that the above results are based on a Chinese high-speed passenger car. The influence of the setup error of the roller rig on stability may be inconsistent with numerical values for other vehicles. However the general trend should be the same.

D. Examples of Comparison Results with Theoretical Analysis

The following are examples of vehicle dynamic tests carried out on the Chengdu roller rig. The test results are compared with theoretical analyses.

FIGURE 14.42 Freight car on the roller rig.

1. Stability Test

a. Stability Tests and Theoretical Analysis of a Freight Car[4]

The first example of a stability test is a heavy haul freight car, designed and manufactured by Qiqihaer Rolling Stock Works. The main purpose of the test was to evaluate the hunting stability and ride performance of the car. The test was carried out in 1995. The freight car on the roller rig is shown in Figure 14.42.

The heavy haul freight car is designed for an axle load of up to 25 t and a maximum speed of 120 km/h, using a three-piece bogie. In order to improve the stability of three-piece bogies, cross-bracing between two side-frames, elastic side bearers, and axle box rubber springs are incorporated in the design. The car body is available in two types, the normal body has a bogie separation of 9.2 m and the other a bogie separation of 7.8 m.

The roller rig speed acceleration or deceleration rate is chosen as 1.25 km/h per second. It has been found through tests that the critical speed for the car with a long car body is approximately 90 to 98 km/h and is approximately 78 to 92 km/h for the car with a short body. The distribution of test results is due to nonlinearities such as friction, clearance, and bump stops. The hunting motion of the wheelset is shown in Figure 14.43. The hunting motions for the front and rear bogie are in opposite directions. When the hunting motion occurs, the flange contact appears, which means the critical speed is V_{C1} (see Figure 14.18). Then, gradually lowering the roller rig speed, the freight car becomes stable at approximately 40 to 50 km/h (see Figure 14.43b), which means the critical speed V_{C2} is very low and cannot meet the design speed. After investigating the suspension parameter, the reasons for low stability are:

- There is longitudinal clearance in the side bearer (of about 1 mm). The side bearer should work longitudinally as a friction damper, but due to the clearance it acts as a spring and cannot provide the intended yaw friction torque.
- The bogie warp stiffness is only 1 MN/rad (design value is 6 MN/rad).
- The longitudinal stiffness of primary suspension is strongly nonlinear due to the structure of the suspension.
- The stiffness value reduces with increasing displacement, which is shown in Figure 14.44.

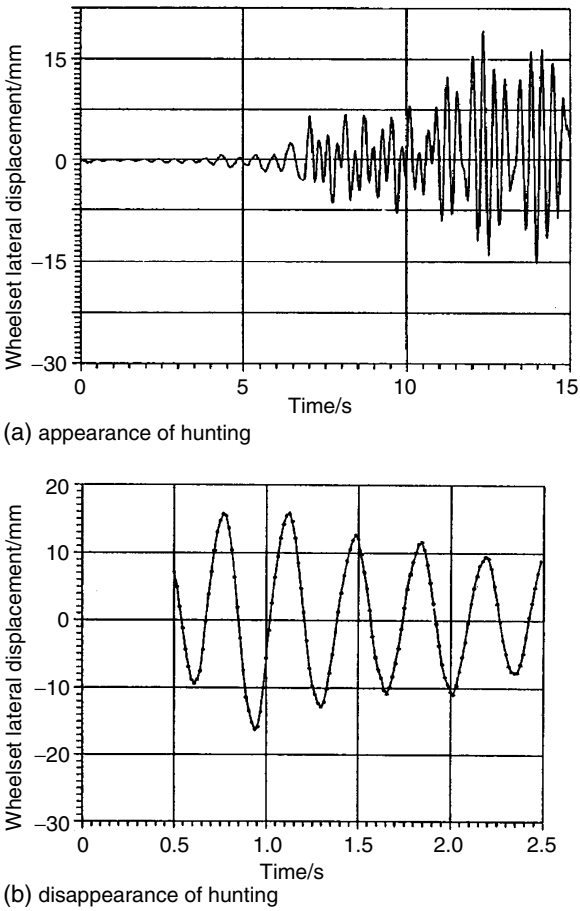

FIGURE 14.43 Record signal of hunting.

The stability of the freight car has been analysed using a simulation method with measured parameters. The degrees of freedom of the freight car are listed in Table 14.5. A total of 44 degrees of freedom are taken into consideration. A nonlinear wheel–roller geometry relationship is used and the object of the simulation is to recreate the stability test process. The start speed is

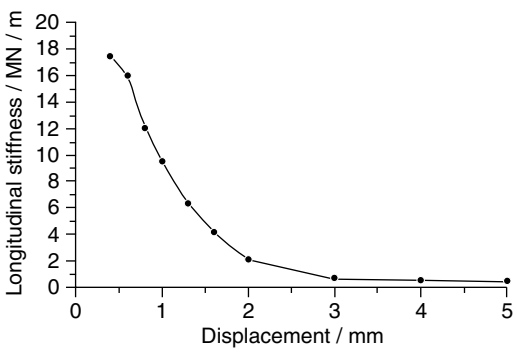

FIGURE 14.44 Longitudinal stiffness.

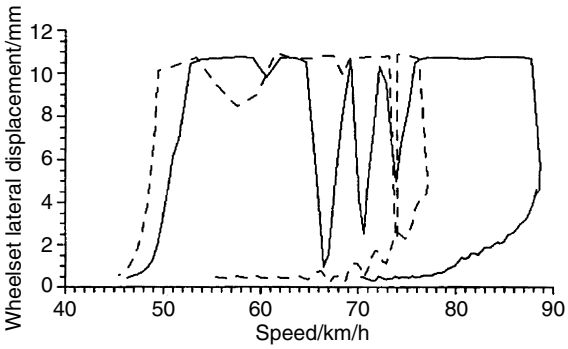

FIGURE 14.45 Wheelset lateral displacement amplitude.

TABLE 14.5
Degrees of Freedom of Freight Car

Coordinate Rigid Body	*X* Longitudinal	*Y* Lateral	*Z* Vertical	θ Roll	φ Pitch	ψ Yaw
Wheelset ($i = 1 \sim 4$)	x_w	y_w			φ_w	ψ_w
Side frame ($i = 1,2$) (r, l)	x_f	y_f	z_f		φ_f	ψ_f
Bolster[a] ($i = 1,2$)						ψ_H
Car body	x_c	y_c	z_c	θ_c	φ_c	ψ_c

[a] Other motions of bolster are considered in car body motions.

70 km/h for the long car-body car and 55 km/h for short car-body car. Figure 14.45 shows the simulation results for the wheelset lateral motion, the solid line is for the long car and the dashed for the short car. It can be seen that the hunting motion at small amplitudes occur at 78 to 88 km/h for the long car and at 70 to 77 km/h for the short car. When the speed is greater than 88 km/h for the long car and 77 km/h for the short car, the hunting motion increases and flange contact occurs. Then, gradually lowering the speed, the system becomes stable at speeds of 53 and 49 km/h for the long car and short car, respectively. Figure 14.46 depicts the hunting motion of wheelset in amplitude and phase. It can be seen that the calculated results correlate well with the test results.

Field testing of the vehicles have shown that the long car becomes unstable at approximately 100 km/h, and after increasing the warp stiffness and improving the side bearers, the freight car can run in service at 120 km/h.

b. Stability Test and Theoretical Analysis of a Passenger Car[31]

A stability test on a passenger car was carried out on the Chengdu roller rig in 1998. The passenger car was manufactured by Hanjin Industry of Korea and was in service on the Heng-guang line in China. The passenger car uses a stainless steel car body made in Korea and the bogies are made in China. Its design speed is 200 km/h. The vehicle is shown on the roller rig in Figure 14.47.

Before the test was undertaken, the stability of the passenger car on rail and on the roller rig was theoretically analysed. The results are shown in Figure 14.48a; the solid line shows the wheelset limit cycle amplitude on rail, and the solid line with a black circle are the results running on the roller rig. It can be seen that the critical speed on the roller rig is lower than on rail, the difference

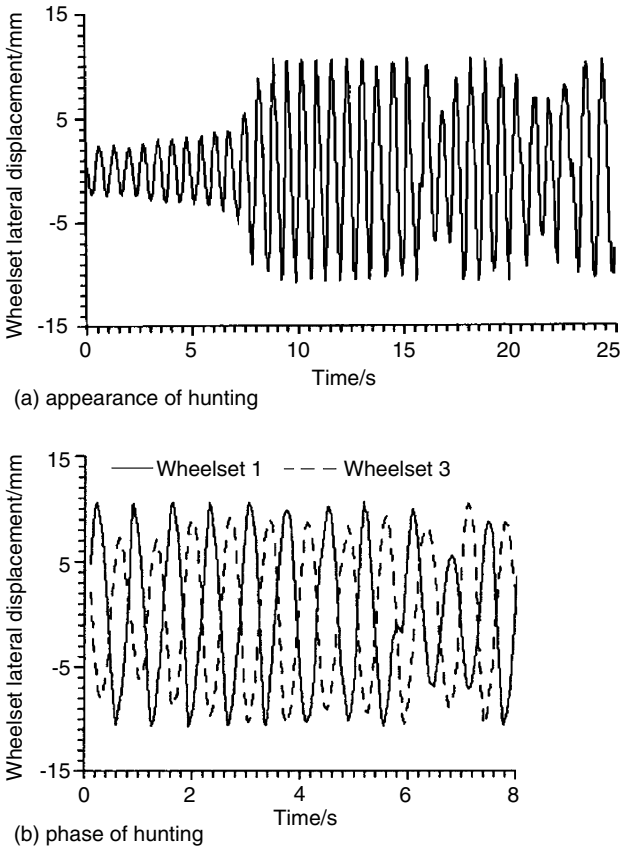

FIGURE 14.46 Hunting motion of calculation: (a) appearance of hunting; (b) phase of hunting.

FIGURE 14.47 Stainless steel car-body passenger car on roller rig.

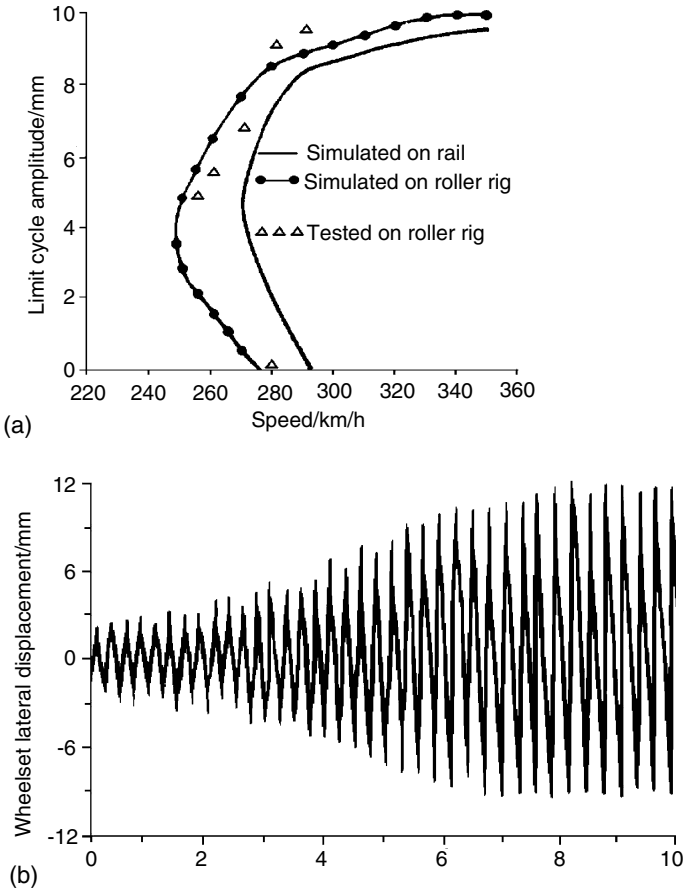

FIGURE 14.48 Wheelset hunting motion: (a) limit cycle amplitude; (b) appearance of hunting motion.

being about 20 km/h. The triangle symbols shown in Figure 14.48a are the test results measured on the roller rig. The measured linear and nonlinear critical speeds are approximately 280 and 255 km/h which correlate quite well with the theoretical values. Figure 14.48b shows that the wheelset hunting motion is very sinusoidal in form. The test results demonstrated the tested passenger car can run at a design speed of 200 km/h.

2. Ride Comfort Test and Theoretical Analysis of a Passenger Car[35,36]

A dynamic performance test on a wide-gauge (1676 mm) coil spring passenger bogie manufactured by the Changchun Car Company was carried out on the Chengdu roller rig in 2002. The test vehicle on the rig is shown in Figure 14.49. The main purpose of the test was to evaluate the hunting stability and ride comfort of the passenger car for use in Pakistan.

The dynamic performance of the vehicle system is also simulated. For simplicity in modelling the complex system, the following assumptions were made:

- The wheelset, bogie frame, and car body are considered as rigid bodies.
- The adjacent vehicles are not considered and only one vehicle is used in the simulation.

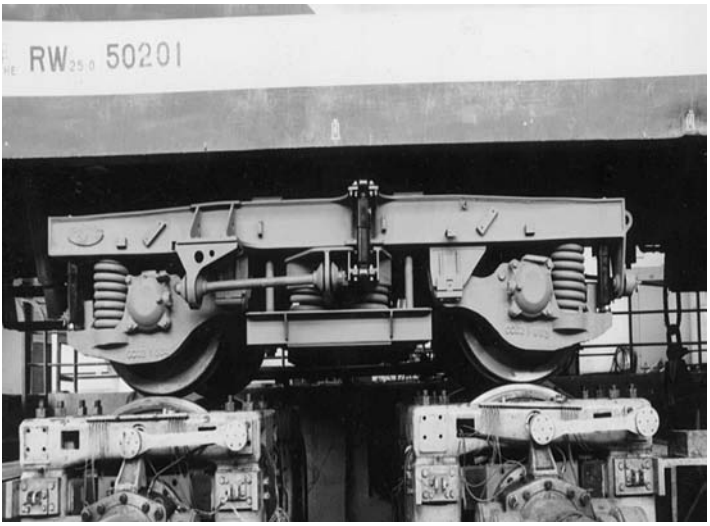

FIGURE 14.49 Wide-gauge passenger car bogie on roller rig.

TABLE 14.6
Degrees of Freedom of the Vehicle System

DOF Body	Lateral	Vertical	Roll	Pitch	Yaw
Car body	Y_c	Z_c	Φ_c	θ_c	ψ_c
Bogie frame	$Y_{b1\sim2}$	$Z_{b1\sim2}$	$\Phi_{b1\sim2}$	$\theta_{b1\sim2}$	$\psi_{b1\sim2}$
Wheelset	$Y_{w1\sim4}$	$Z_{w1\sim4}$	$\Phi_{w1\sim4}$	—	$\psi_{w1\sim4}$

The total number of degrees of freedom of the vehicle system, which is listed in Table 14.6, is 31.

The dynamic simulation program TPLDYNA, developed by the State Key Laboratory of Traction Power, was used for the dynamic performance computations of the vehicle on rail. The

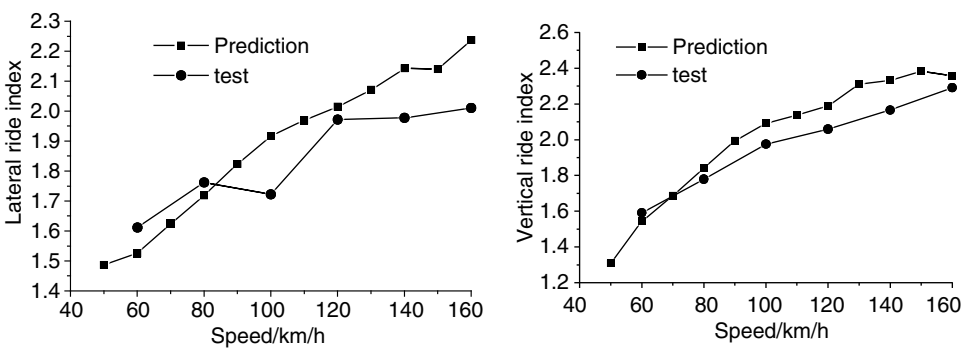

FIGURE 14.50 Comparison of test results and theoretical predictions.

stochastic irregularities of the U.S.A. grade 5 track irregularity spectrum was used in the dynamic simulation and also for ride comfort testing on the roller rig.

Through the simulation and test, the vibration accelerations on the car body were determined. The ride index calculation method is in accordance with Chinese national standard GB5599-85 (Railway Vehicles Specification for evaluation of the dynamic performance and accreditation test).

The lateral and vertical ride indices of the test and theoretical predictions, at different speeds, are shown in Figure 14.50. It can be seen that the test results are a little lower than the simulation results when at higher running speeds.

VI. CONCLUSIONS

From a brief historical review of roller test rigs for railway vehicles, it can be seen that roller rigs have played an important role in railway history, especially in the development of high-speed trains. Roller rigs are very useful in the testing of railway vehicles for the purpose of examining dynamic performance, estimating and optimising parameters, checking capabilities in extreme situations (e.g., high speed, violent impact), etc. Although the roller rig is becoming increasingly complex, in order to simulate vehicle running accurately, the inherent errors in wheel–rail contact must always be considered and these lead to test results for hunting speed, vibration response (ride index) and wheel–rail force under curve simulation which can differ from field tests. For this reason, roller rigs cannot replace field testing. Now some famous roller rigs (such as the roller rigs in Derby, Pueblo, and Munich) have been decommissioned, it could be said that the golden age for roller rigs has passed. The reason is probably that roller rigs have already taught us many things and knowledge has increased with respect to vehicle design, structures, and performance. Additionally, as simulation techniques become more advanced the need for costly testing plants diminishes. Since the roller rig is useful in developing high-speed trains, they will still be used in developing countries such as China.

REFERENCES

1. Jaschinski, A., Chollet, H., Iwnicki, S., Wickens, A., and Von Würzen, J., The application of roller rigs to railway vehicle dynamics, *Vehicle Syst. Dyn.*, 31, 345–392, 1999.
2. Anon, Locomotive testing plant at Sweden, *The Engineer*, 100, 621–622, 1905.
3. Carling, D. R., Locomotive testing stations, parts 1 and 2, *Trans. Newcomen Soc.*, 45, 105–182, 1972.
4. Weihua, Z., *Dynamic Simulation Study of Railway Vehicle*, Ph.D. Dissertation, Southwest Jiaotong University, P.R. of China, 1996, June.
5. Ma, S. J., Zhang, W. H., Chen, G. X., and Zeng, J., Full scale roller rig simulation for railway vehicles, 13th IAVSD Symposium of Vehicles on Roads and Tracks, Chengdu, P.R. of China, August 1993, *Vehicle Syst. Dyn.*, 23(Suppl.), 346–357, 1994.
6. Deutsche Bahn, A. G., Welte Druck GmbH, Central Division for Research and Testing Research and Test Centre 3 *The Roller Rig*, Munich-Freimann, 1994, December.
7. Rizzi, C. and De Luca, S., La sala sperimentazione veicoli ferroviari del centro ricerche ansaldo transporti. *Ingegneria Ferroviaria*, 48(7), 459–464, 1993, in Italian.
8. Vitrano, F. and Ghislanzoni, F., Descrizione della sala sperimentazione veicoli ferroviari. *Ingegneria Ferroviaria*, 48(7), 465–479, 1993, in Italian.
9. Vitrano, F., Pasten, L., and Flego, U., Le prove su veicoli ferroviari mediante banco a rulli. *Ingegneria Ferroviaria*, 48(7), 480–492, 1993, in Italian.
10. Hoshiya, S., Rolling stock testing plant capable of testing at a speed of 450 km/h, *Jpn. Rail. Eng.*, 102, 12–15, 1987.
11. Miyamoto, M., JR rolling stock testing plant capable of testing at a speed of 500 km/h, *Q. RTRI*, 32(4), 211–212, 1991.

12. Iwnicki, S. D. and Shen Z. Y., Collaborative railway roller rig project, *Proceedings of the SEFI World Conference on Engineering Education*, Portsmouth, p. 255, September 1992.
13. Cooperrider, N. K., Law, E. H., Fries, R. H., and Haque, I., *State-of-the-Art-Car (SOAC), creep forces and dynamic response on the Roll Dynamics Unit*, Arizona State University, Department of Mechanical and Aerospace Engineering, Report CR-R 82037, 1982 September.
14. Fries, R. H., *Estimation of transit rail vehicle parameter from roller rig tests*, Ph.D. Dissertation, Arizona State University, 1983.
15. Fries, R. H., Dynamic response of a transit rail vehicle on a roller rig, The Dynamics of Vehicle on Road and Tracks, Eighth IAVSD Symposium of Vehicles on Roads and Tracks, Cambridge, MA, August 15–19, 1983, *Vehicle Syst. Dyn.*, 13, 1984.
16. Fries, R. H., Cooperrider, N. K., and Law, E. H., Experimental investigation of freight car lateral dynamics, *J. Dyn. Syst., Meas., Control*, 103, 201–210, 1981.
17. Matsumoto, A., Sato, Y., Nakata, M., Tanimoto, M., and Qi, K., Wheel–rail contact mechanics at full scale on the test stand, *Wear*, 191, 101–106, 1996.
18. Dreher, G., Jobst, F., Götz, G., Mauer, L., Meinke, P., Mielcarek, A., Nestmeier, J., and Örley, H., Active hunting control of a wheel/rail vehicle demonstrated up to 530 km/h on the German roller test rig, The Dynamics of Vehicle on Road and Tracks. Eighth IAVSD Symposium of Vehicles on Roads and Tracks, Cambridge, MA, August 15–19, 1983, *Vehicle Syst. Dyn.*, 13, 1984.
19. Elkins, J. A. and Wilson, N. G., Train resistance measurements using a roller rig, The Dynamics of Vehicle on Road and Tracks, Ninth IAVSD Symposium of Vehicles on Roads and Tracks, Linköping, Sweden, June, 1985, *Vehicle Syst. Dyn.*, 15, pp. 86–99, 1986.
20. Dai, H. Y., Robust Performance Analysis of Active Suspension with model Uncertainty Using Structured Singular Value, μ approach, 13th IAVSD Symposium of Vehicles on Roads and Tracks, Budapest, Hungary, August 1997, *Vehicle Syst. Dyn.*, 29(Suppl.), pp. 635–647, 1998.
21. Haque, I. and Law, E. H., Steady state techniques in creep force estimation: results from full scale tests of the SOAC vehicle on a roller rig, *J. Dyn. Syst., Meas., Control*, 111, 61–68, 1989.
22. Francesco, B., Stefano, B., and Ferruccio, R., Wear of railway wheel profiles: a comparison between experimental results and a mathematical model, 17th IAVSD Symposium of Vehicles on Roads and Tracks, Lyngby, Denmark, August 2001, *Vehicle Syst. Dyn.*, 37(Suppl.), pp. 478–489, 2003.
23. Zhang, W. H., Chen, J. Z., Wu, X. J., and Jin, X. S., Wheel/rail adhesion and analysis by using full scale roller rig, *Wear*, 22253(1–2), pp. 82–88, 2003.
24. Eisaku, S. and Masayuki, M., Geometrical contact between wheel and roller rig, *Nippon Kikai Gakkai Ronbunshu, C Hen/Transactions of the Japan Society of Mechanical Engineers, Part C*, 59(562), 1686–1693, 1993.
25. Keiji, Y., Norio, F., and Tatsuro, S., Fundamental consideration of geometrical contact between wheel and rail, *Nippon Kikai Gakkai Ronbunshu, C Hen/Transactions of the Japan Society of Mechanical Engineers, Part C*, 56(528), 2132–2138, 1990.
26. Zhan, W. H. and Chen, L. Q., A study of wheel–roller contact relations on rail vehicle roller rig system, *J. Southwest Jiaotong Univ.*, 30(1), 76–91, 1995, in Chinese.
27. Zhan, F. S., Locomotive Dynamics, Issue: Publishing Company of Chinese Railway, 1990, (in Chinese).
28. Zhang, W. H. and Chen, L. Q., Analysis of difference of rail vehicle stability on track and on roller rig, *J. China Rail. Soc.*, 19(1), 32–36, 1997.
29. De Pater, A.D., The motion of a railway wheelset supported by a pair of rollers as compared with the motion of such a wheelset along a tangent track, Delft University of Technology, Laboratory for Engineering Mechanics, Report 1012, 1993.
30. Dukkipati, R. V., Analysis of the lateral stability of a Track on NRC curved track simulator, *J. Southwest Jiaotong Univ.*, 1994.
31. Zeng, J., Zhang, W. H., Dai, H. Y., Wu, X. J., and Shen, Z. Y., Hunting instability analysis and H_∞ controlled stabilizer design for high speed railway passenger car, 13th IAVSD Symposium of Vehicles on Roads and Tracks, Budapest, Hungary, August 1997, *Vehicle Syst. Dyn.*, 29(Suppl.), pp. 655–668, 1998.
32. Yan, J. M., Wang, K. W., and Dai, H. Y., A Study of the high speed passenger bogies utilizing the full scale roller testing rig, *Vehicle Syst. Dyn.*, 23(Suppl.), 554–565, 1993.

33. Dukkipati, R.V., Parametric study of the lateral stability of a rail bogie on a roller rig, Proceedings of the Institution of Mechanical Engineers, Part F, *J. Rail Rapid Transit*, 213(1), pp. 39–47, 1999.
34. Zhang, W. H., Influence of roller rig state errors to rail vehicles stability testing results, *Chinese J. Mech. Eng.*, 33(3), 49–53, 1997.
35. Wu, P. B., *Dynamic Performance Computations for the Pakistan Wide-Gauge Passenger Car*, Research Report, No. TPL2001-09, State Key Laboratory of Traction Power, Southwest Jiaotong University, P.R. of China, September 2001.
36. Zeng, J. and Dai, H. Y., *Dynamic Performance Test for the Pakistan Wide-Gauge Coil Spring Bogie of Passenger Car Using Roller Testing Rig*, Research Report, No. TPL2002-09, State Key Laboratory of Traction Power, Southwest Jiaotong University, P.R. Of China, May 2002.